Mechanisms of Photocurrent Generation at Metal and Semiconductor Electrodes

Thesis by

Harry Osborn Finklea

In Partial Fulfillment of the Requirements

for the Degree of

Doctor of Philosophy

California Institute of Technology

Pasadena, California

1976

(Submitted August 1, 1975)

For me there is only the traveling on paths that have heart, on any path that may have heart. There I travel, and the only worthwhile challenge is to traverse its full length. And there I travel looking, looking, breathlessly.

Don Juan

from The Teachings of Don Juan
by Carlos Castaneda

ACKNOWLEDGMENTS

First of all, I would like to thank my advisor, Joseph G. Gordon, for his patience and inspiration during these long years of wandering in the wilderness. His wife, Ruth, deserves a hat tip for her equally inspired cooking. Fred Anson, with his incisive questions and unerring logic, revealed many a gap in my thinking, and initiated me into the mysterious rites of electrochemistry. A pitcher of beer is dedicated to Harry Gray, who demonstrated that chemists, if not chemistry, can be fun. All of the faculty at Caltech, and especially the chemistry faculty, have provided me with a better understanding and appreciation of high quality scientific research. Thanks are due to Dr. Nicolet, Joe Feng, and Joe Harris, who assisted me in the preparation of the thin-metal film electrodes and Hall effect measurements. I am grateful for the financial support offered by Caltech, IBM, and the Shell Oil Company. Edi Bierce gets an ovation for her superb typing, an sample of which you are now reading. Finally, I dedicate this thesis to my mother, as partial compensation for the task of raising me.

ABSTRACT

An attempt to measure the electrochemical properties of an excited molecule is made. Polyaromatics and $Ru(bipy)_3^{2+}$ are photoexcited in nonaqueous electrolytes via a monochromatic beam passing through a thin-metal film electrode. It is concluded that observation of charge transfer from an excited molecule is not possible because of rapid quenching by energy transfer to the electrode. All observed photocurrents in the presence of a light-absorbing solute are explained by heating of the solution near the interface or the photochemical generation of electroactive products. Anodic and cathodic photocurrents are observed in the absence of a dye. The mechanism of the latter process entails the formation of excited holes and electrons within the metal with their subsequent reaction at the interface. Photoelectron ejection into the solution is also proven by the effects of an electron scavenger.

A related problem is the mechanism of dye-sensitization at a semiconductor electrode. The concentration dependence of the photoinduced oxidation of the dye rhodamine 6G at a polycrystalline SnO_2 electrode is determined in aqueous and nonaqueous electrolytes. In water, the concentration study reveals a slow irreversible buildup of an adsorbed dye layer. Photocurrent spectra suggest that the

sensitizing species is the monomer within the adsorbed layer, slightly perturbed by its environment. The adsorbed layer structure is hypothesized to be localized in clumps. In acetonitrile, onset of sensitization does not occur until 10^{-4} M dye concentrations are reached. Over the next decade of concentration, the photocurrent caused by excitation of the electrode decreases by a factor of two, indicating the formation of a uniform monolayer. Evidence for sensitization by non-adsorbed molecules is obtained. Again, dilution reveals an irreversible adsorption process. The observation of fluorescence quenching of the adsorbed dye as a function of electrode potential is attempted. The negative results are attributed to the low quantum yield of the sensitized photocurrent.

TABLE OF CONTENTS

TABLE OF CONTENTS (Cont'd)

LIST OF FIGURES

PART I: The Origin of Photocurrents at Metal Electrodes in Nonaqueous Solvents

INTRODUCTION

The initial impetus for this research was provided by a brief communication from Crow and Aggarwal[1]. They reported the photo-assisted reduction of nickel(II) complexes at dropping and pool mercury electrodes. By applying a constant potential corresponding to the foot of the Ni(II) reduction wave and focusing an intense monochromatic beam onto the electrode surface, large photocurrents appeared at wavelengths strongly absorbed by the nickel complexes. Two figures were included which showed excellent correlation between the photocurrent spectra of $Ni(H_2O)_6^{2+}$ and $Ni(en)_3^{2+}$ and their absorption spectra. However, an additional uv band was shown which does not really appear in the solution absorption spectra of these complexes[2]. Their results seemed to corroborate earlier findings by Durst and Taylor[3], who observed a photo-induced "pre-wave" when scanning the potential into the reduction wave of $Ni(H_2O)_6^{2+}$. The proposed mechanism consisted of an initial promotion of electrons from the bonding t_{2g} orbitals to the antibonding e_g orbitals. The population of e_g orbitals then lead to a weakening of the metal-ligand bonds, causing a

lowering of the activation energy for reduction. Alternatively, electron promotion provided vacant orbitals at lower energy for electron transfer. In either case, the excited complex is reduced at a less negative potential than the ground-state molecule.

Crow's second paper [4] amended the earlier results. Plots of the photocurrent versus potential for various metal ions produced polarogram-like curves that resembled the dark current polarograms. Similar results were obtained by us for aqueous Ni^{2+} and Cd^{2+} (Fig. I-1). More surprising was the wavelength dependence of the photocurrent obtained by Crow. Zn^{2+}, Cu^{2+}, Ni^{2+}, Co^{2+}, Mn^{2+}, Cr^{2+}, VO^{2+}, Ca^{2+}, and Cd^{2+} all exhibited a similar photocurrent spectrum when the DME was held at the diffusion-limited reduction potential for each respective ion. The spectrum contained 5 to 6 peaks between 425 and 725 mμ, with some variation in intensity and position for different metal ions. Crow hypothesized that the large electric field near the electrode distorted the d orbitals into approximately the same configuration for all of the ions; Cd^{2+} and Ca^{2+} required the invocation of similar splitting in unfilled f and d orbitals. At those wavelengths, we believe that a more likely explanation is that a strong heating of the electrode-solution interface produces convection currents, increasing the rate of transport of reducible ions to the electrode. The photocurrent spectrum is then a function of energy flux; in Crow's

experiments, photocurrents were not normalized to a constant flux. At higher photon energies, electrons are photo-ejected from the electrode into the solution; Martinus et al.[5] proposed the catalytic scavenging of aquated electrons by Ni^{2+}, even when Ni^{2+} reduction was diffusion-limited, by the reaction sequence:

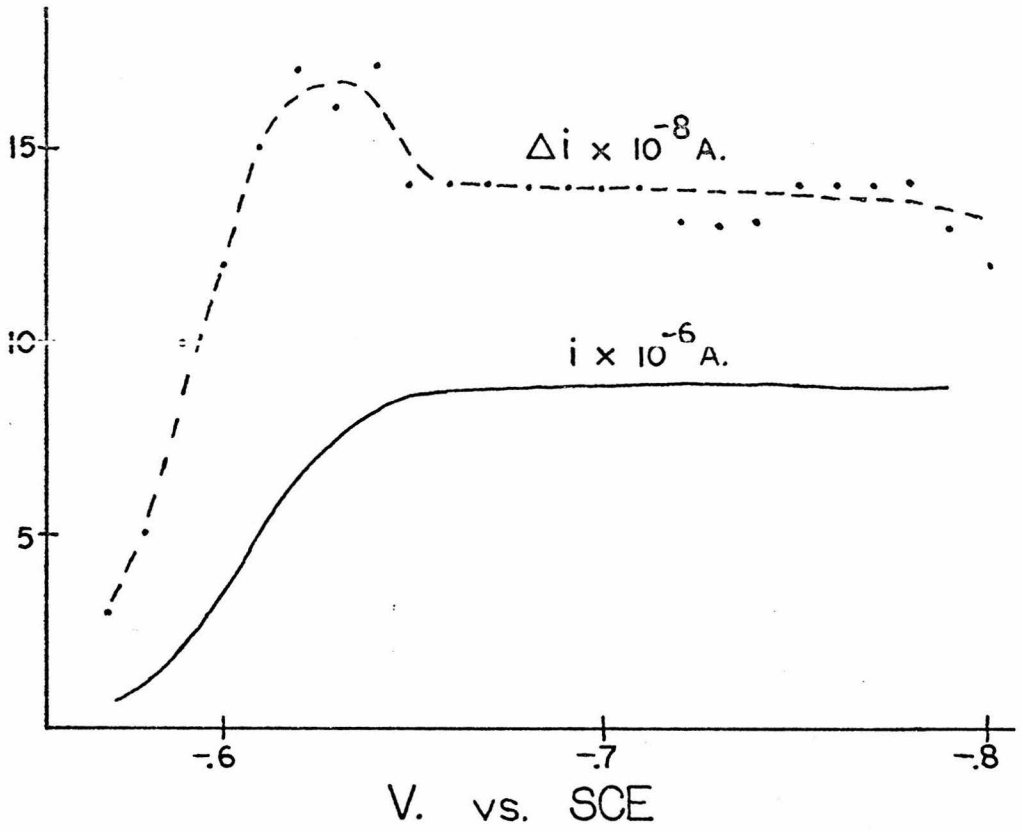

Fig. I-1. Cd^{2+} Photocurrent

i -- Peak dark current at a DME

Δi -- Increase of peak current during illumination

$$e^- \text{(metal)} \xrightarrow{h\nu} e^- \text{(aq)}$$

$$e^- \text{(aq)} + Ni^{2+} \longrightarrow Ni^{+}$$

$$Ni^{+} + H_2O \longrightarrow Ni^{2+} + H + OH^-$$

$$H \longrightarrow H \text{ (adsorbed)}$$

$$H \text{ (adsorbed)} + H_2O + e^- \longrightarrow H_2 + OH^-$$

However, the idea of investigating electrochemical properties of excited molecules still seemed like a good one; it was merely a question of optimizing conditions for the observation of electron transfer from the excited state. One needed a molecule with a high molar absorbance and a long-lived excited state, such as anthracene and other cyclic aromatics. Furthermore, the exciting light should pass through the electrode to maximize intensity at the electrode surface. The latter condition required an optically transparent electrode (OTE), of which there were three varieties: thin metal films, gold grids, and commercial SnO_2 semiconductor electrodes. The narrow available potential range of solid electrodes in water and the low aqueous solubility of polyaromatics then led to the use of non-aqueous solvents; acetonitrile proved to be optimal from the photochemical and electrochemical standpoint. As oxygen rapidly quenched the long-lived triplets, vacuum line techniques were used to rigorously exclude it from the system.

In Part I, results obtained with thin metal-film electrodes are reported; work with the SnO_2 electrodes has been allocated to Part II. The initial surprising discovery was the existence of background photocurrents, obtained in the absence of any dye. Especially puzzling was the presence of anodic (electrons moving from the solution into the electrode) photocurrents as well as cathodic ones. When light-absorbing molecules were added to the solution, additional photocurrents were observed at wavelengths corresponding to the absorption bands of the molecules, but it was not at all clear that these photocurrents were caused by direct electron transfer from photo-excited molecules.

Several arguments against the observation of excited state electron transfer can be presented. The excited molecule is presumed to be more easily reducible and more easily oxidizable than the ground state molecule by arguments similar to those presented for Ni^{2+}; hence, for maximum sensitivity, the electrode is maintained at a potential between the first oxidation and reduction waves of the unexcited molecule where only the excited species reacts. If, for example, the electrode transfers an electron into an excited molecule, the ground state anion, or more accurately, the one-electron reduction product is produced. However, the electrode potential, being less negative than the reduction potential, causes rapid

re-oxidation of the reduced product, generating the ground state molecule with no net photocurrent. There is a possibility that the reduction product could diffuse away from the electrode surface before re-oxidation occurred. A theoretical treatment [6] of just such a process predicted a maximum photocurrent of 10^{-12} A/cm^2 for excited state lifetimes (τ) of 10^{-7} sec and rapid electron-transfer rates. Since the magnitude of the photocurrent depended on the square root of τ, not much could be gained by increasing the excited state lifetime.

Even more probable than the double-electron step process is the quenching of excited states by rapid energy transfer to the metal. Experiments [7-9] with dyes spaced at various distances from a metal surface by fatty acid layers have shown strong fluorescence quenching occurring within 100 Å of the surface. Consequently, an excited molecule diffusing toward the electrode would be de-excited at distances too great for electron transfer.

Killesreiter and Baessler [10] did prove the existence of charge transfer from singlet excitons in an anthracene crystal to a metal film deposited on or near the crystal surface. Energy transfer quenching occurred simultaneously. Prock and Zahradnik [11] studied the photoconduction of pyranthrene in benzene at both metal and tin oxide electrodes. The postulated photocurrent mechanism included

the generation of ions from the bimolecular reaction of an excited pyranthrene molecule with an unexcited molecule prior to charge transfer with the electrode. The only report of photocurrents in a conventional electrochemical system with a metal electrode demonstrated that the origin of the photocurrents were photochemical reactions producing electroactive species [12]. The systems were platinum or amalgamated gold electrodes in contact with aqueous solutions of rhodamine B or fluorescein. The electrode had to be cathodically polarized initially to produce the doubly-reduced leuco-dye. The following reaction scheme was proposed:

$$D + h\nu \longrightarrow D^* \longrightarrow {}^3D$$

$${}^3D + DH_2 \longrightarrow 2\dot{D}H$$

$$\dot{D}H \longrightarrow D + H^+ + e^-$$

where D is the ground state dye, D^* the excited singlet state, ${}^3D$ the triplet state, DH_2 the leuco-dye, and $\dot{D}H$ the semi-reduced radical. Addition of reducing agents also produced the same anodic photocurrents. The most convincing evidence that the photocurrents were caused by photochemical products diffusing to the electrode was the slow rise and decay times of the photocurrents for step pulses of light. In fact, the decay times were matched with the decay of an absorption transient due to radicals.

Despite the evidence against the observation of excited-state electrochemistry, experimentation was continued to elucidate the mechanisms of the photocurrents in nonaqueous solvents.

EXPERIMENTAL

Electrodes

Working electrodes consisted of a thin film of platinum vapor-deposited on a quartz substrate. Annealing the electrodes in an oven seemed to prevent the film from chipping and pealing while in contact with solution. Typical properties were: resistance 20-50 Ω/square, optical density 0.5-1.3, thickness approximately 100 Å. Some gold and platinum thin film electrodes were purchased from Harrick Scientific Corporation and used without annealing. Representational absorption spectra are shown in Fig. I-2.

Vacuum electrochemical techniques

Two vacuum-tight electrochemical cells were employed (Fig. I-3). Cell #2 had superior noise characteristics and a shorter time response to transient stimuli. The working electrode was epoxied with TORR-SEAL to the body of the cell. The reference and counter electrodes were isolated by two asbestos fiber tips and a medium fritted disc, respectively. A silver wire was used as a quasi-reference electrode, or dried silver perchlorate was placed in the reference electrode compartment to form an Ag^+/Ag couple when solvent was added. The potential assumed by the reference electrode

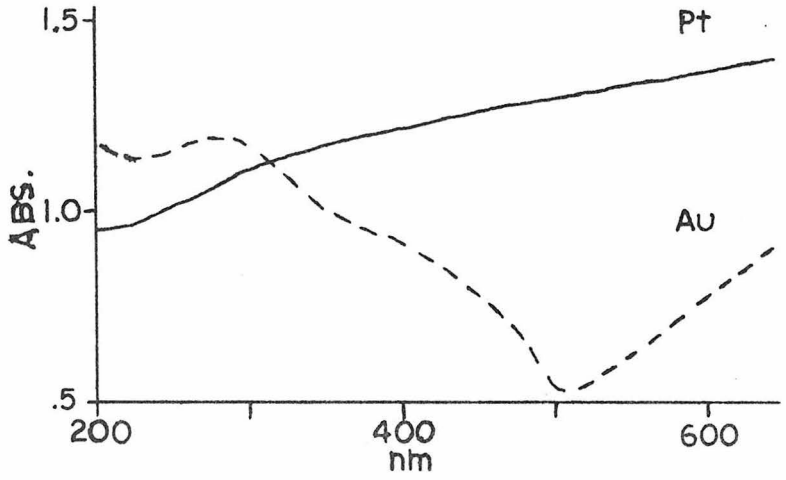

Fig. I-2. OTE Absorption Spectra

Fig. I-3. Electrochemical Cells

W -- working electrode
R -- reference electrode
C -- counter electrode
I -- indicator electrode

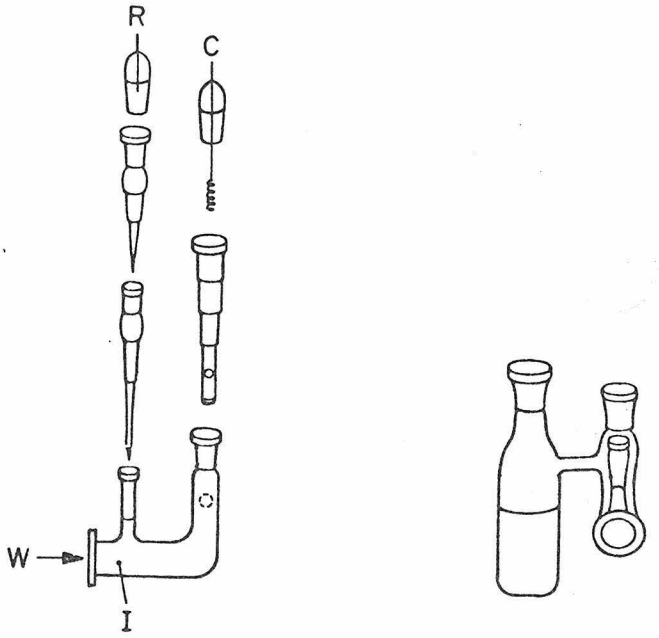

CELL #1

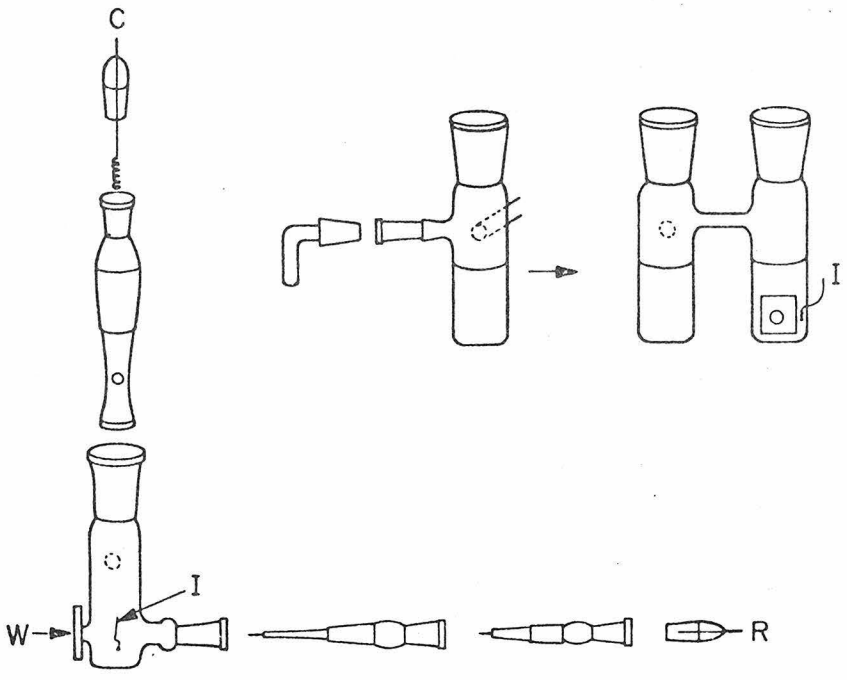

CELL #2

was measured by the position of half-wave potentials of reversible couples, e.g., $Ru(bipy)_3(ClO_4)_2$, or by placing a saturated NaCl calomel electrode in the cell at the end of the experiment. The cell was prepared by charging the sidearm with supporting electrolyte, evacuating the cell overnight, and vacuum-distilling solvent into the sidearm up to a calibrated mark. The resulting solution was degassed with three freeze-thaw cycles using an oil diffusion pump. After pouring the solution into the electrochemical cell, the cell was filled with de-oxygenated argon to atmospheric pressure to force solution into the reference electrode compartment, and sealed. A uniform $AgClO_4$ solution was produced by agitation with a micro-stirring bar. The counter electrode compartment was filled through a hole in its side. A short length of platinum wire functioned as an indicator electrode during the cyclic voltammograms used to monitor the electrochemistry. A small sidearm contained solid chemicals which could be added during the course of the experiment without breaking the seal.

Chemicals

Acetonitrile exhibited the optimal properties of low solution resistance and low light absorption down to 200 mμ. Purification consisted of vacuum-distillation of spectroquality acetonitrile

(Matheson, Coleman, and Bell) onto freshly activated alumina and then into the cell. N, N′-dimethylformamide was fractionally distilled twice from calcium hydride under a nitrogen atmosphere (15 torr). 1, 2-dimethoxyethane was dried with the benzophenone anion generated by sodium metal.

Supporting electrolytes were recrystallized five times from distilled water and vacuum-dried. Solutions were usually 0.1 M tetraethylammonium perchlorate in acetonitrile.

Anthracene (blue fluorescence grade), 9, 10-diphenylanthracene, and laser-grade rhodamine 6G chloride were purchased and used without further purification. Tris(bipyridyl)ruthenium(II) complex and acridine orange dye were converted to perchlorate salts and recrystallized.

Photocurrent measurements

Because of the extremely small size of the photocurrents, the cell was placed inside a Faraday cage along with a battery-powered potentiostat (Fig. I-4) to eliminate power line noise. Measurements were always made at a constant applied potential. The photocurrent was converted to a voltage and monitored with an oscilloscope or with a lock-in amplifier synchronized with a light chopper. A 1000-watt mercury-xenon lamp was focused through a 10 cm water filter onto

Fig. I-4. Battery-Powered Potentiostat

W -- to working electrode
R -- to reference electrode
C -- to counter electrode
I.V. - input voltage
G -- case ground

The operational amplifier as a Burr-Brown 3521J (FET imput, low noise, low power). The 9 V. batteries are standard transistor power cells; the 2.7 V. source contains two mercury cells connected in series.
Resistances are in ohms.

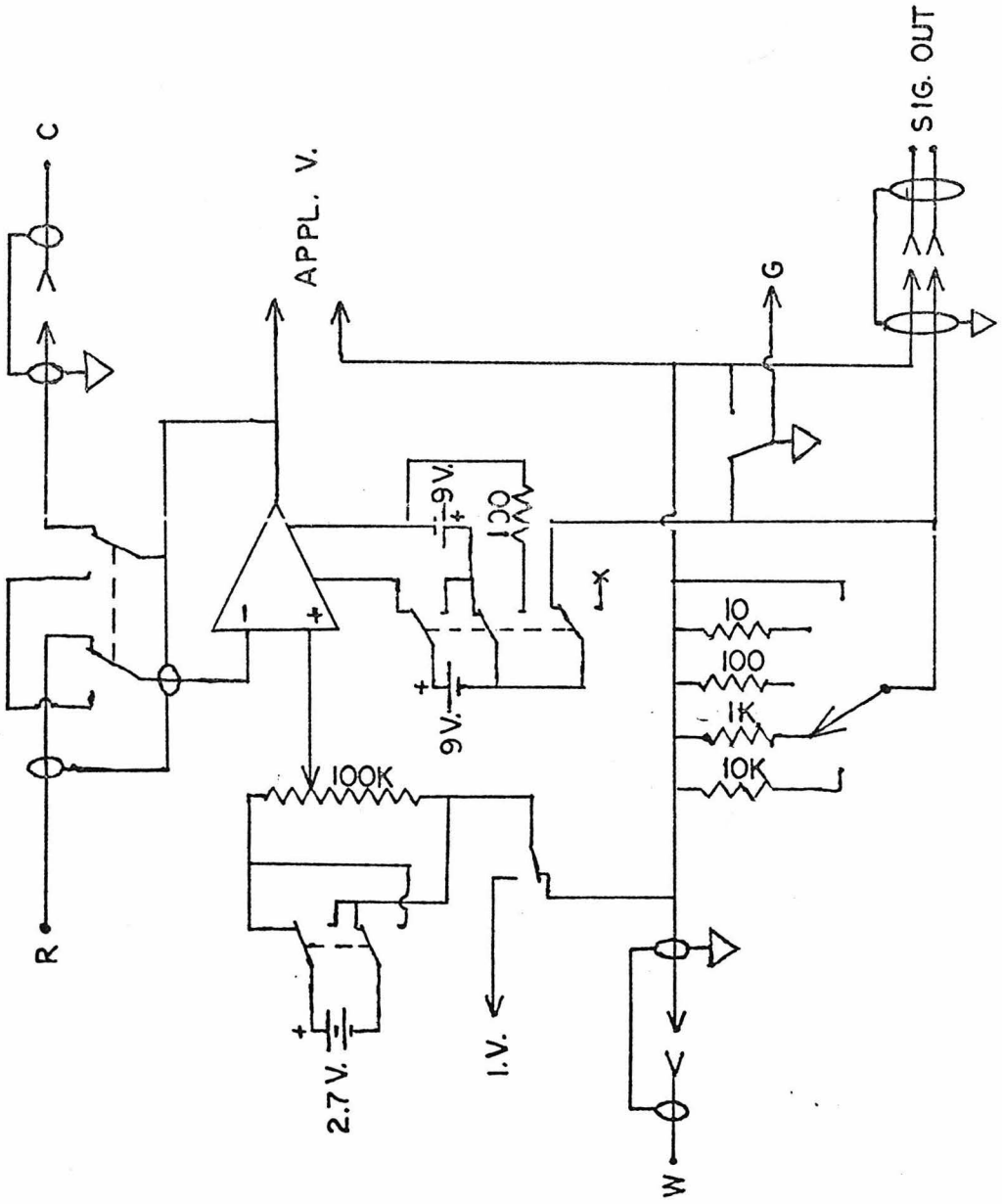
C
APPL. V.
G
SIG. OUT
9V.
100
X
10
100
1K
10K
100K
9V.
R
2.7 V.
I.V.
V
W

the entrance slit of a Jarrel-Ash #82-410 monochromator. The exiting beam, filtered to remove higher order spectra, was focused through a shutter, the light chopper, and a hole in the side of the Faraday cage (Fig. I-5). The beam passed through the working electrode and into the solution. Intensity of the beam was calibrated with a thermopile (Fig. I-6). Photocurrent data was corrected to a constant light intensity, assuming that the photocurrent was proportional to intensity. When a narrow bandpass was used, fluctuations in the corrected photocurrent occurred around the mercury line wavelengths where strong variations in intensity were present (Fig. I-6). The fluctuations were attributed to the different wavelength response of the thermopile and the photocurrent.

Fig. I-5. Optical Excitation Apparatus

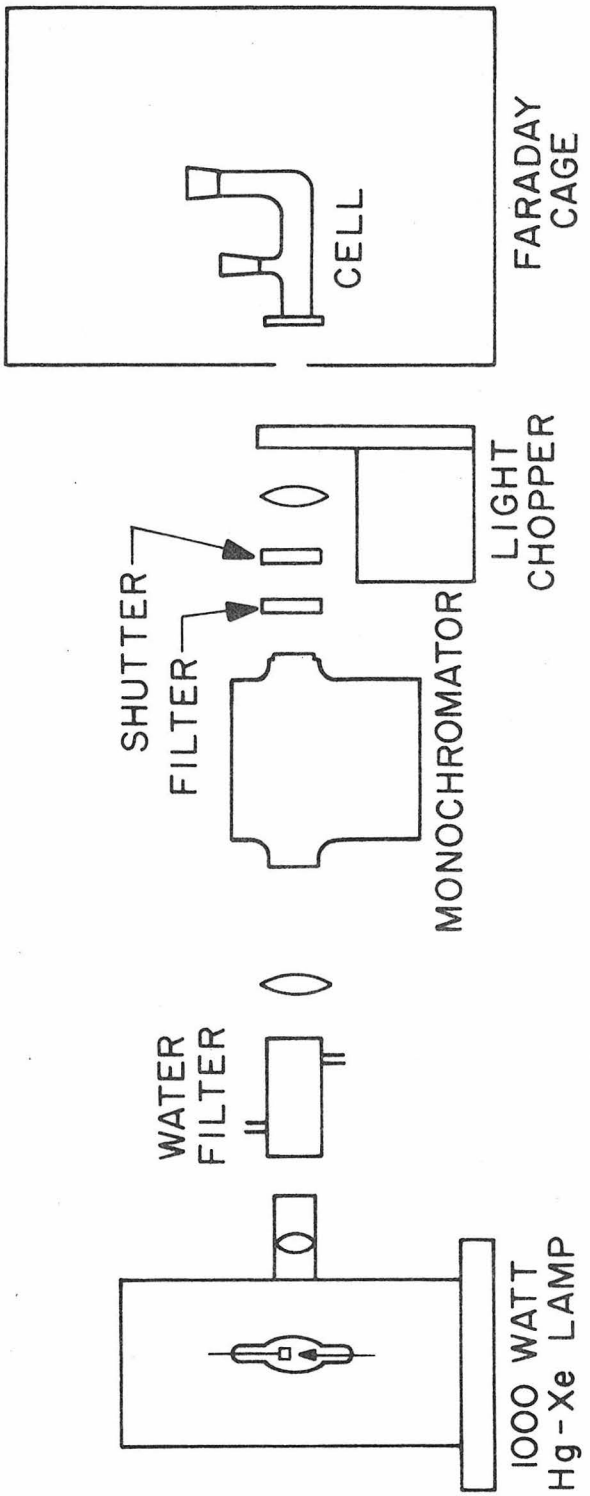
1000 WATT
Hg-Xe LAMP
WATER
FILTER
SHUTTER
FILTER
MONOCHROMATOR
LIGHT
CHOPPER
CELL
FARADAY
CAGE

Fig. I-6. Excitation Beam Intensity

——— 7 mμ bandpass; $\times 10^{15}$ photons/sec/cm^2

- - - - 33 mμ bandpass; $\times 10^{16}$ photons/sec/cm^2

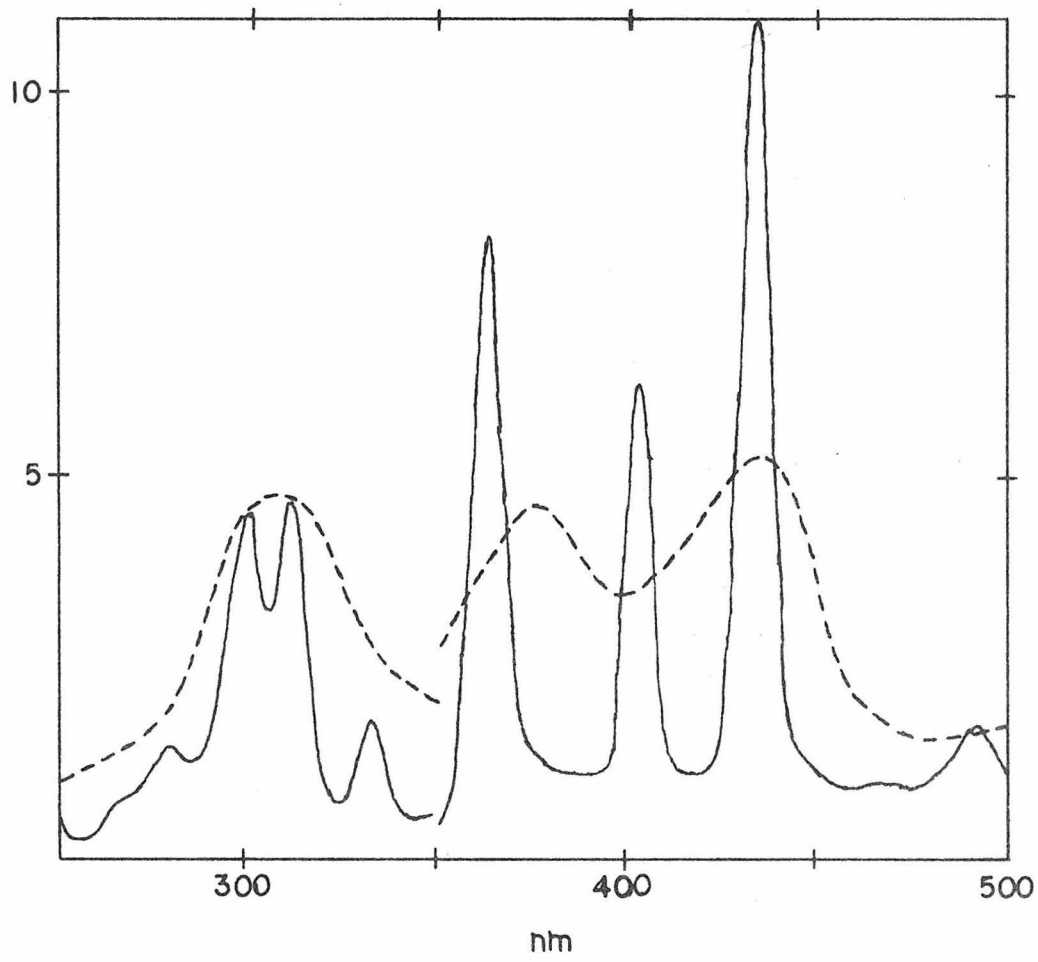
10
5
300
400
500
nm

RESULTS AND DISCUSSION

Background photocurrents

Figure I-7 shows the wavelength dependence of the background photocurrent at a series of constant potentials. The qualitative features were independent of solvent (acetonitrile, N,N-dimethylformamide, and dimethoxyethane), supporting electrolyte (TEAP, $NaClO_4$, and $NaBF_4$), and metal (platinum and gold). The solvents and supporting electrolytes were transparent (absorbance $< .01$) over most of the spectral region in Fig. I-7, so the hypothesis of an unknown impurity photochemically reacting to form an electroactive product seems unlikely. The photocurrent quantum yield was low enough that an impurity that efficiently converted each photon absorbed into an electron crossing the interface could have an extremely low absorbance. For example, a photon flux of 10^{15} photons/sec at the electrode-solution interface produced a maximum photocurrent of roughly 100 nA. The solution absorbance calculated for a 1:1 photon-electron conversion process is then .0003. But in order to account for the short risetime of the photocurrent (vide infra), the lifetime of the photo-activated species must be 10^{-4} sec or less. Assuming a diffusion coefficient of 10^{-5} cm^2/sec, the photo-activated must then be within $\sqrt{D\tau}$, or

Fig. I-7. Background Photocurrent

The reference electrode was a Ag/Ag^+ couple, measured to be +.32 V vs SCE. Photocurrent magnitude is in arbitrary units.

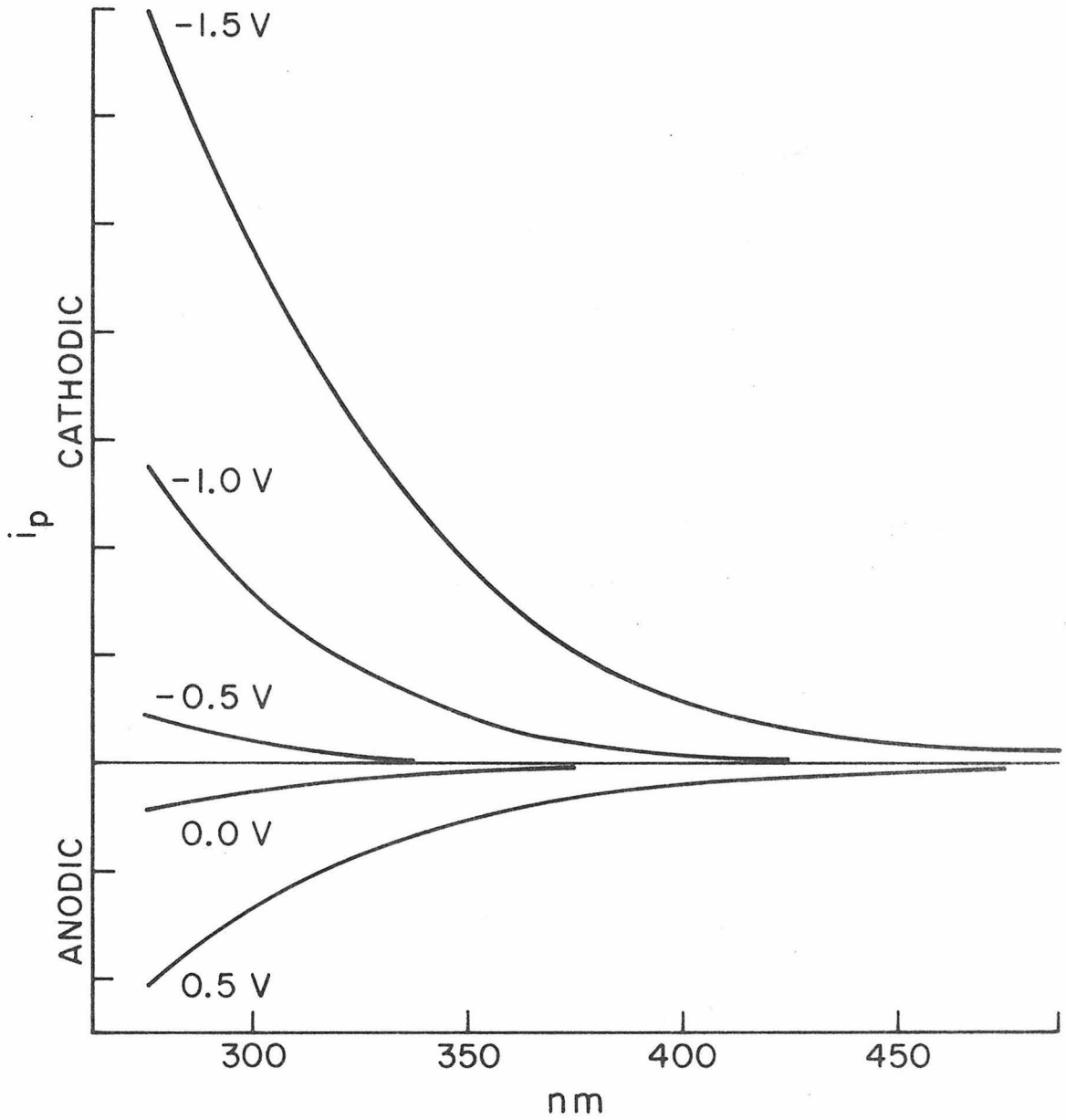
-1.5 V
-1.0 V
-0.5 V
0.0 V
0.5 V
i_p
CATHODIC
ANODIC
300
350
400
450
nm

3×10^{-5} cm of the electrode; therefore, the solution absorbance per centimeter is 10, clearly not a transparent solution. One must resort to an adsorbed layer. However, the existence of the same photoelectrochemically active adsorbed impurity in all of the systems listed above is improbable. A more plausible origin is the metal electrode, which absorbs 70% to 95% of the light incident on the cell (Fig. I-2).

Heating of the electrode at the electrolyte interface can cause changes in the double-layer structure and charge density for a short time after the onset of illumination[13]; at longer times convection currents are produced that increase the flow of electroactive impurities to the electrode surface. An increase in solution temperature also affects the diffusion rates; a typical diffusion coefficient changes 2%/°C, leading to a 1% change in the current. Heating photocurrents are thus characterized by slow rise and decay times. In contrast, the background photocurrents exhibited rise and decay times equivalent to the charging time constant of the cell (Fig. I-8), i.e., $i_p = k(1 - e^{-t/\tau})$ or $k(e^{-t/\tau})$ where τ is the characteristic RC cell constant. The equivalent circuit of the potentiostat-cell combination is shown in Fig. I-9. Given the conditions that V is constant and $R_f \gg R_s$, then a sudden change in R_f causes an exponential change in the current as observed in Fig. I-8, where $\tau = R_s C_d$. The physical process which changes the faradaic resistance must reach a

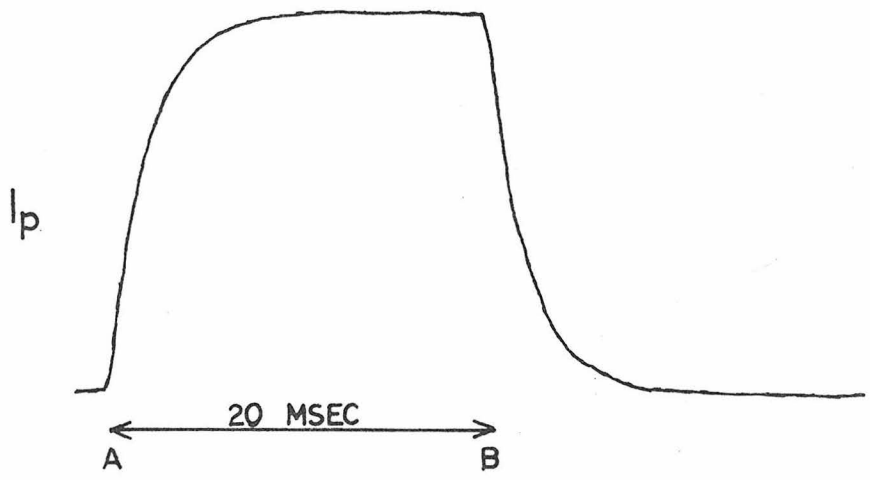

Fig. I-8. Time Dependence for Short Intervals

Chopping frequency, 25 Hz

A -- light on; B -- light off

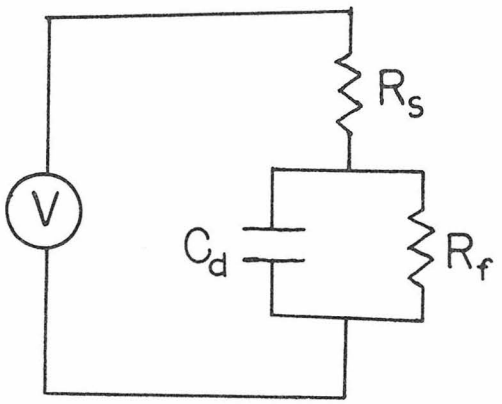

C_d -- double-layer capacitance

R_s -- uncompensated solution resistance

R_f -- faradaic resistance

V -- constant applied potential

Fig. I-9. Equivalent Circuit for Cell-Potentiostat

steady-state value much faster than the cell RC constant. For a 0.1 M TEAP/CH_3CN solution, τ for cell #1 was typically 2 msec, for cell #2, 0.5 msec. Such a rapid and reproducible response discourages the hypothesis that the photocurrents are caused by heating of the electrode-electrolyte interface.

The wavelength dependence of the photocurrent (Fig. I-7) was also inconsistent with heating effects. Temperature changes should be proportional to the energy flux absorbed by the electrode, which in turn is proportional to the electrode optical absorbance. The platinum OTE absorbance decreased with decreasing wavelength (Fig. I-2); one would then predict a drop in the photocurrent for shorter wavelengths. However, when the λ response was normalized to constant energy flux, rather than intensity, the photocurrents still rose with decreasing λ.

A comprehensive body of experiments [13-27] have proven that mercury electrodes (and, in one case, silver [28]) can photo-eject electrons into a solvent when irradiated at photon energies well below the metal work function. Subsequent irreversible scavenging of the solvated electrons produces a net cathodic photocurrent. Theoretical treatment of potential and wavelength dependence yields $I_p \propto (h\nu - eV - h\nu_0)^n$, where n is either 2 [21] or 5/2 [29]. Most authors have plotted $I_p^{1/n}$ versus the applied potential to check linearity.

The presence of sizable anodic photocurrents at more positive potentials, which obviously cannot be produced by photoelectron ejection, makes the photon energy plot more certain in ascertaining whether the cathodic photocurrents can be attributed to photoemission. Indeed, quite linear plots were obtained for both exponents (Fig. I-10a), but with significantly different extrapolated threshold wavelengths. However, the anodic photocurrents also produced linear plots (Fig. I-10b), with $I_p^{2/5}$ giving a slightly better fit to a straight line. Consequently a further test for solvated electrons was necessary. All published experiments had used an electron scavenger, a compound which reacts irreversibly with the solvated electron and prevents its return to the electrode. Two of the most commonly used scavengers were nitrous oxide and protons. But before effects of these compounds on the background photocurrent are described, the time and history dependence of the photocurrent will be discussed.

The background photocurrent exhibited a slow decay over a period of seconds (Fig. I-11); also a subsequent measurement always yielded a lower magnitude for constant wavelength and potential. This phenomenon was particularly evident at high photocurrent densities. The initial magnitude and even the direction of the photocurrent depended on prior history of the electrode. For example, in Fig. I-12 a "cyclic voltammogram" of the photocurrent was obtained by changing

Fig. I-10. $i_p^{1/n}$ vs. Photon Energy

a -- cathodic photocurrents

Intercepts: n = 2, 2.90 eV (428 mμ)
n = 5/2, 2.71 eV (457 mμ)

b -- anodic photocurrents

Intercepts: n = 2, 2.28 eV (544 mμ)
n = 5/2, 1.97 eV (629 mμ)

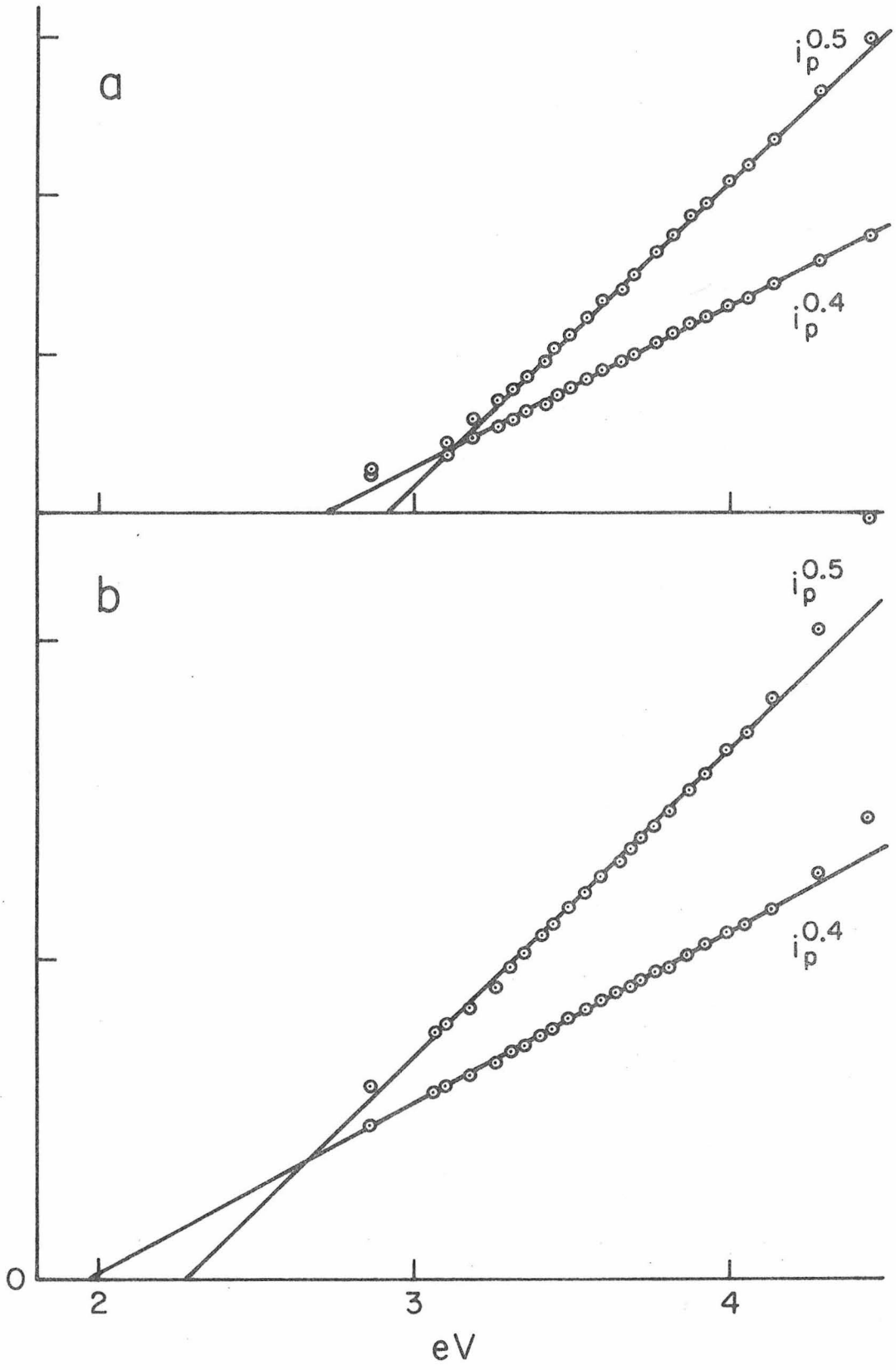
a
$i_p^{0.5}$
$i_p^{0.4}$
b
$i_p^{0.5}$
$i_p^{0.4}$
0
2
3
4
eV

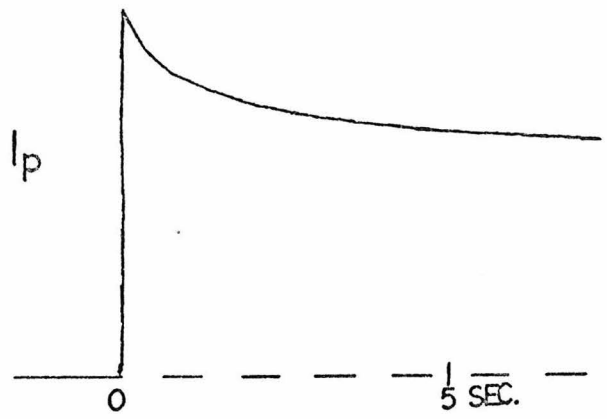

Fig. I-11. Time Dependence for Long Intervals

Hand-operated shutter

the potential 0.1 V between each measurement; three complete cyclic scans were performed to check reproducibility. A large hysteresis was evident; in particular the zero-crossover point depended on the direction of the scan. At any given potential, the photocurrent became more anodic (less cathodic) after the potential had been scanned to more negative potentials, and more cathodic (less anodic) after a scan to more positive potentials.

Gerischer et al.[28,30] have also observed anodic photocurrents upon irradiation of a metal electrode in contact with a nonabsorbing electrolyte. His proposed mechanism furnishes the best explanation for the results presented above (Fig. I-13). Light of sufficient energy

Fig. I-12. Background Photocurrent Potential Scan

Photocurrent in nA. Positive values indicate cathodic current. The potential of the reference electrode vs. SCE is +.39 V.

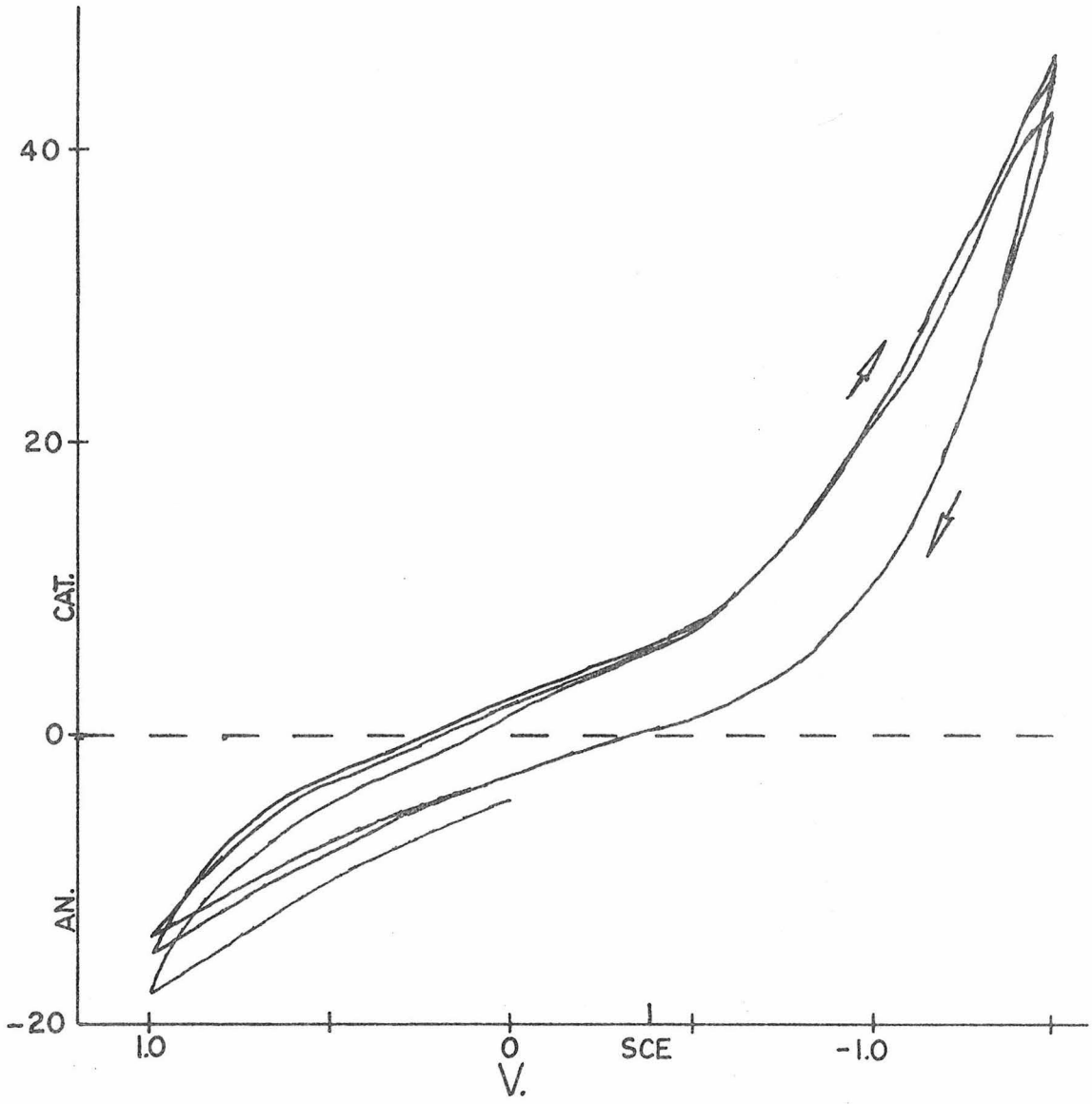
40
20
0
-20
CAT.
AN.
1.0
0
SCE
-1.0
V.

Fig. I-13. Reaction Pathways for Excited Holes and Electrons

A -- acceptor; D -- donor;
P -- product; E_f -- Fermi level

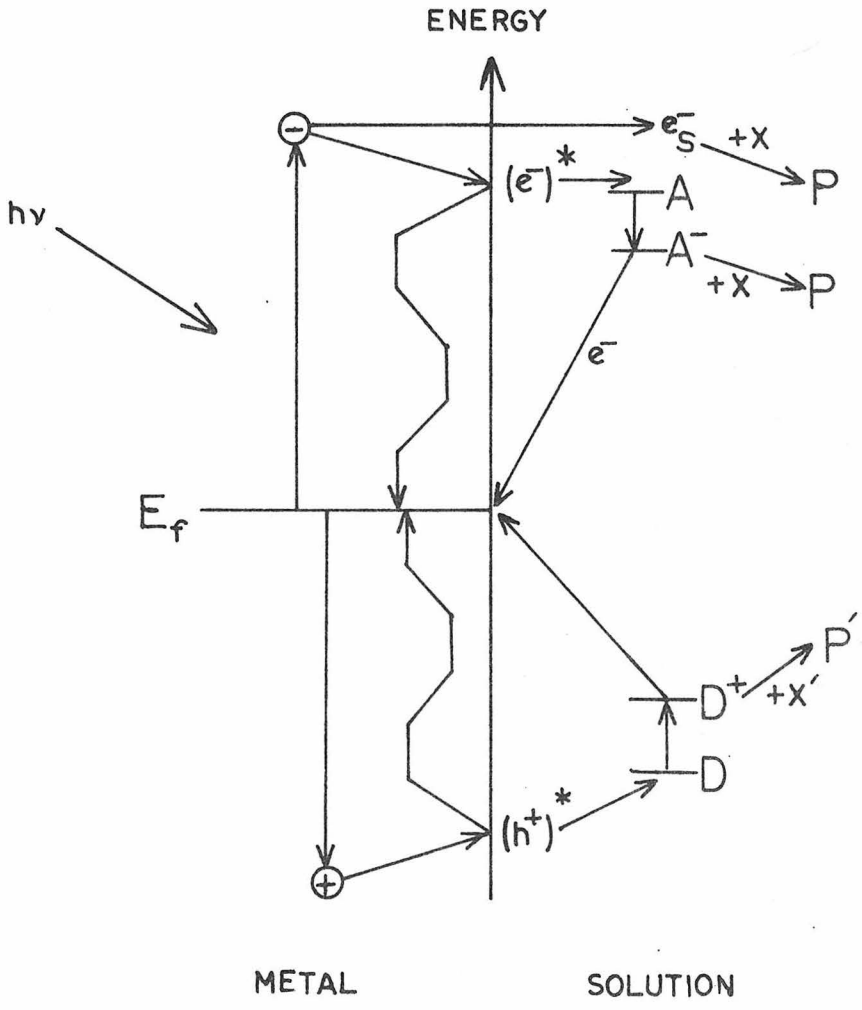
ENERGY
hν
e^-_s
+X
P
$(e^-)^*$
A
A^-
+X
P
e^-
E_f
D^+
+X'
P'
D
$(h^+)^*$
METAL
SOLUTION

absorbed by the metal produces a separation of electrons and holes, the electrons occupying the vacant levels above the Fermi level, and the holes existing below it. These excited holes and electrons have greater oxidizing and reducing potential, respectively, than the electrode normally has at the applied potential, and are sufficiently mobile and long-lived that they can react with electrochemical couples at the surface of the electrode. Photocurrent is produced when the electron transfer is irreversible, as in a rapid subsequent chemical reaction of the donor or acceptor molecule. Photoemission is also possible if the electron acquires sufficient kinetic energy in the direction normal to the surface. A change in the applied potential to a more positive value lowers the Fermi level of the metal relative to energy levels in the electrolyte, increasing the probability of the excited hole oxidizing a donor level. Cathodic polarization yields the analogous effect for excited electrons. In the systems studied, the maximum photocurrent quantum yield, obtained at the extreme negative potential, was 10^{-3} to 10^{-4}, calculated for photons absorbed by the electrode. Maximum anodic photocurrents were approximately one quarter as large. These values are comparable to results obtained by Gerischer[30].

The photocurrent decayed with time because of slow consumption of the irreversible couples near the electrode. However,

electrolysis at very negative potentials increased the concentration of donor levels, so that when the potential was returned to an intermediate value, the photocurrent became more anodic. The opposite process was even more striking; enormous cathodic photocurrents were observed at 0.0 V (Fig. I-12) after prolonged electrolysis at more positive potentials.

The identity of the donor and acceptor molecules is uncertain. In aqueous solution, Gerischer[30] postulated that H_2O was irreversibly oxidized by the excited hole:

$$h^+ + H_2O \longrightarrow \dot{O}H^*_{ads} + H^+ \longrightarrow O_{ads} + 2H^+ + e^-$$

The hydroxyl radical was sufficiently excited that a second electron was donated into the metal above the Fermi level. A corresponding pH change was observed during irradiation.

Even in nonaqueous media, water is still a possible scavenger for holes and electrons. The existence of a monolayer of water molecules is consistent with the comparable quantum yields obtained in water and acetonitrile. However, if one calculates the consumption rate of monolayer of water at the maximum photocurrent levels, less than 1% of a monolayer per second is destroyed, e.g., a water monolayer contains 10^{15} molecules/cm^2, and a photocurrent of 1 μA/cm^2 is

less than 10^{13} electrons/sec/cm^2. Yet at these current levels, a rapid decay over the initial few seconds is observed.

The results of the scavenging experiments can now be presented. In Fig. I-14, the background photocurrent "cyclic" was obtained; then N_2O was bubbled through the solution. A significant increase in the cathodic photocurrent was noted. Sweeping the solution with argon lowered the cathodic photocurrent, thus confirming the presence of photo-ejected electrons which normally diffused back to the electrode. In another experiment, addition of p-toluenesulfonic acid proved to be inconclusive because proton reduction in the dark severely limited the accessible potential range. The analogous experiment for holes was attempted by the addition of the azide ion. The overall reaction is:

$$2N_3^- + 2h^+ \longrightarrow 3N_2$$

Low solubility in CH_3CN required the use of N, N-dimethylformamide as solvent. No significant enhancement of anodic photocurrents was observed, indicating that the mechanism was different, or the rate was limited by the kinetics of hole production, reaction, and recombination, rather than the concentration of donor molecules.

Fig. I-14. Effect of Nitrous Oxide on the Background Photocurrent

——— 0.1 M TEAP/CH_3CN; Ar saturated

– – – after bubbling with N_2O

• • • after bubbling with Ar

photocurrent in nA.

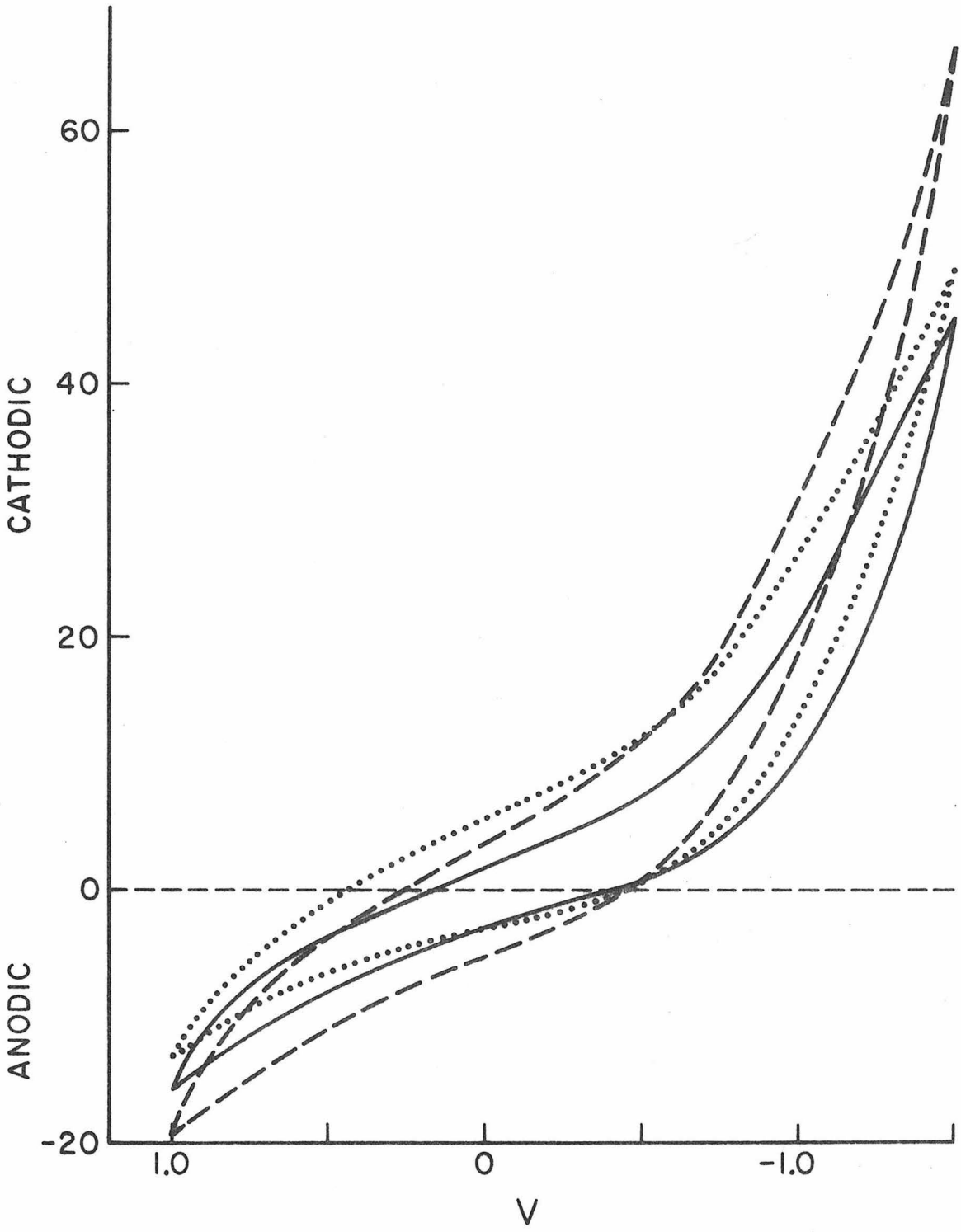
60
40
20
0
-20
CATHODIC
ANODIC
1.0
0
-1.0
V

Dye-sensitized photocurrents

The earliest experiments were performed with 10^{-3} molar anthracene or $Ru(bipy)_3^{2+}$. As shown in Fig. I-15 the photocurrent was enhanced at wavelengths strongly absorbed by the dye. The risetimes in these results were not measured. It is conceivable that excited molecules near the electrode surface were transferring their energy to the metal, increasing the rate of formation of holes and excited electrons, and thus increasing the magnitude of the background photocurrent. However, when the concentrations were raised to 10^{-2} M for both anthracene and $Ru(bipy)_3^{2+}$, slow rise and decay times appeared (Fig. I-16) which were characteristic of heating currents or of photochemical reactions producing electroactive species in the bulk[31]. For anthracene, a known photochemical reaction in high dielectric solvents is the production of free ions from bimolecular triplet encounters[32]. Although these ionic charge carriers have a lifetime of roughly 10^{-4} sec, they could further react to form electroactive products. Another complication arises from the photodimerization reaction of anthracene, which occurs at high solution concentrations and light intensities[33]. The 9,10-diphenyl derivative of anthracene is not susceptible to dimerization reactions[34], and has a considerably lower triplet yield[35]. Again, slow rise and decay times were observed in a 10 mM solution. These photocurrents were

Fig. I-15. Dye Sensitized Photocurrents

(a) -- 1 m$\underline{M}$ anthracene
(b) -- 1 m$\underline{M}$ $Ru(bipy)_3^{2+}$

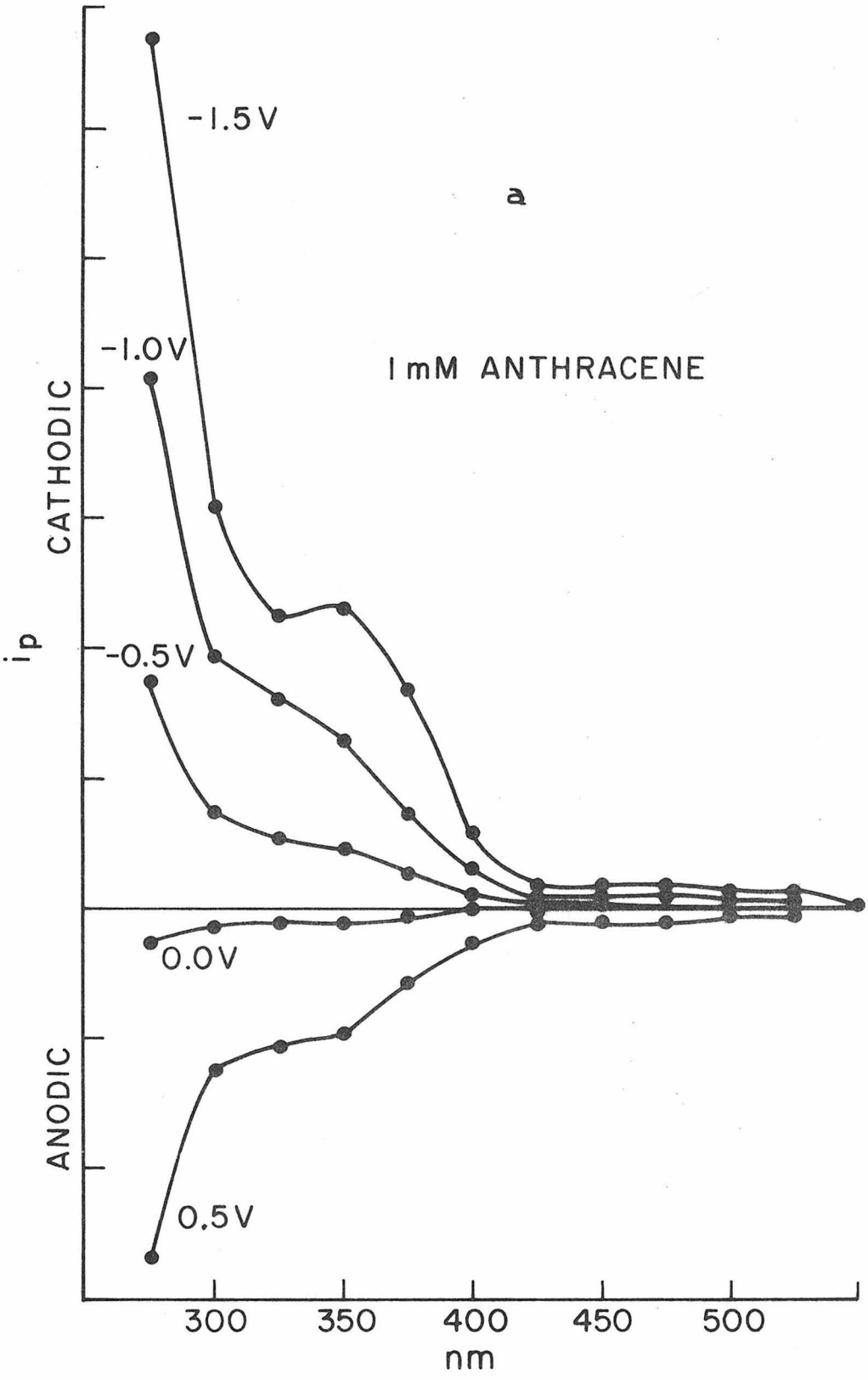
-1.5V
a
-1.0V
1 mM ANTHRACENE
CATHODIC
i_p
-0.5V
0.0V
ANODIC
0.5V
300
350
400
450
500
nm

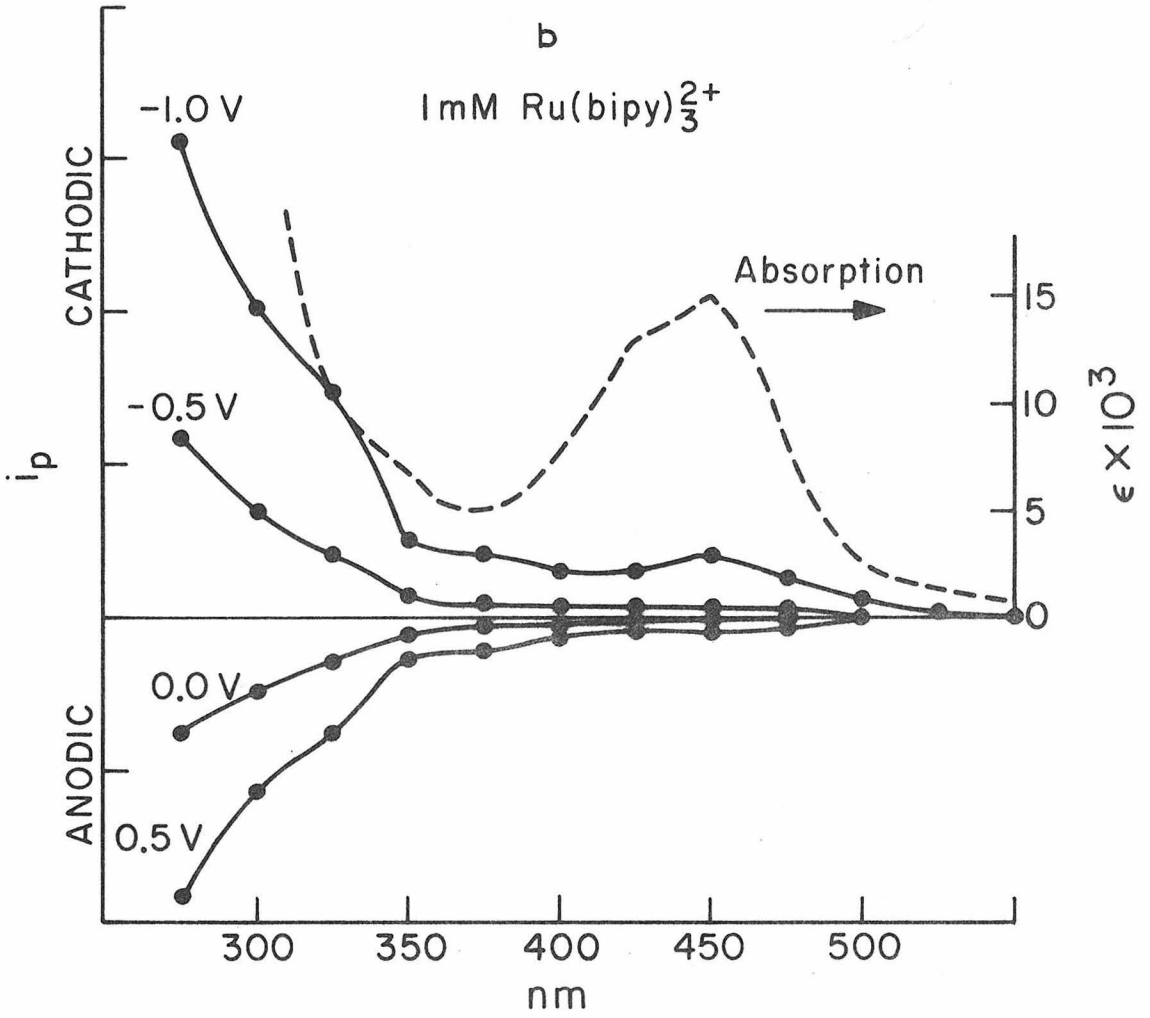
b
1mM Ru(bipy)$_3^{2+}$
-1.0 V
-0.5 V
0.0 V
0.5 V
CATHODIC
ANODIC
i_p
Absorption
15
10
5
0
$\epsilon \times 10^3$
300
350
400
450
500
nm

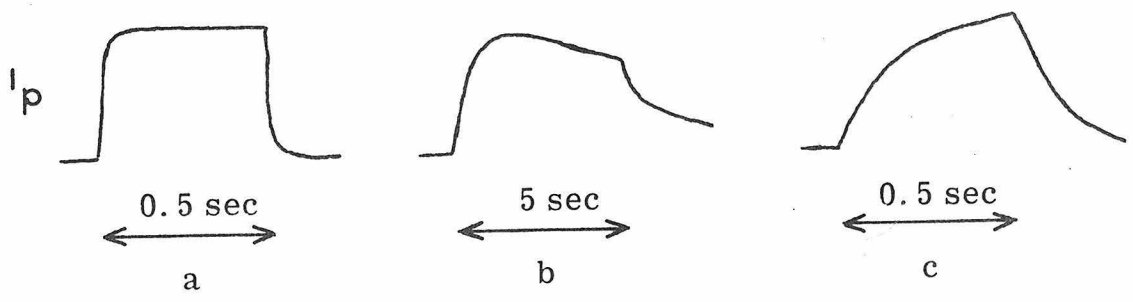

Fig. I-16. Comparison of Background Photocurrent Risetimes with Photochemical Photocurrents

Shutter risetimes 0.01 sec.

(a) -- background photocurrent
(b) -- 10 mM anthracene
(c) -- acridine orange; rhodamine 6G

attributed to heating effects. The dyes acridine orange and rhodamine 6G have absorption band peaks well into the visible (496 mμ and 526 mμ, respectively) where the background photocurrent is extremely small. Although acridine orange photocurrents exhibited fairly rapid risetimes ($\sim$10 msec) at one particular potential, much slower responses were noted at all other potentials (Fig. I-16). Rhodamine 6G photocurrents were consistently anodic, with extremely slow rise and decay time.

In summary, there is no persuasive evidence for the observation of electron transfer between a metal electrode and a photoexcited molecule in solution, i.e., electrochemistry of the excited state. All observed photocurrents can be attributed to (1) heating of the electrolyte at the interface, (2) photo-production of electrochemically active species, or (3) excitation of the electrode. The basic difficulty lies in the continuum of energy levels, both filled and empty, within the metal. The probability of energy transfer quenching of the dye is high no matter what its excitation energy is. Electron transfer quenching has been demonstrated for $Ru(bipy)_3^{2+}$, where the excited complex donated an electron to an acceptor with discrete energy levels, e.g., an easily reduced molecule [36]. Energy transfer was prevented by choosing the electron acceptor to have a higher excited state energy than the Ru complex. By comparing the rate constant for emission quenching with the reduction potential of a series of acceptors, a half-wave potential of -0.81 V vs. SCE was derived for the $Ru(bipy)_3^{3+}/Ru^*(bipy)_3^{2+}$ couple [37]. The difference between this value and the $Ru(bipy)_3^{3+}/Ru(bipy)_3^{2+}$ couple (+1.29 V) is 2.10 V, which compares rather nicely with the 2.18 eV energy of the triplet energy of the Ru(II) complex. All of the excitation energy appears to act as the driving force for electron transfer.

REFERENCES

1. D. R. Crow and P. K. Aggarwal, Chem. Commun., 780 (1969).
2. F. A. Cotton and G. Wilkinson, "Advanced Inorganic Chemistry", Interscience, 2nd ed., 1966, p. 882.
3. R. A. Durst and J. K. Taylor, J. Res. N.B.S., 69A, 517 (1965).
4. D. R. Crow and S. L. Ling, J.C.S. Dalton Trans., 698 (1972).
5. N. Martinus, D. M. Rayner, and C. A. Vincent, Electrochim. Acta, 18, 409 (1973).
6. J. M. Hale, J. Phys. Chem., 73, 3196 (1969).
7. H. Kuhn, J. Chem. Phys., 53, 101 (1970).
8. R. R. Chance, A. Prock, and R. Silbey, J. Chem. Phys., 60, 2184 (1974).
9. R. R. Chance, A. Prock, and R. Silbey, J. Chem. Phys., 60, 2744 (1974).
10. H. Killesreiter and H. Baessler, Chem. Phys. Lett., 11, 411 (1971).
11. A. Prock and R. Zahradnik, J. Chem. Phys., 49, 3204 (1968).
12. R. Memming and G. Kürsten, Ber. Bunsenges. Physik. Chem., 76, 4 (1972).
13. G. C. Barker, B. Stringer, and M. J. Williams, J. Electroanal. Chem., 51, 305 (1974).

14. G. C. Barker, G. Bottura, G. Cloke, A. W. Gardner, and M. J. Williams, J. Electroanal. Chem., 50, 323 (1974).

15. G. C. Barker, Ber. Bunsenges. Physik. Chem., 75, 728 (1971).

16. G. C. Barker, A. W. Gardner, and D. C. Sammon, J. Electrochem. Soc., 113, 1182 (1966).

17. G.C. Barker, Electrochim. Acta, 13, 1221 (1968).

18. R. de Levie and J. C. Kreuser, J. Electroanal. Chem., 21, 221 (1969).

19. M. Heyrovsky, Proc. Roy. Soc. London, A301, 411 (1967).

20. M. Heyrovsky, Nature, 206, 1356 (1965).

21. V. P. Sharma, P. Delahay, G. G. Susbielles, and G. Tessari, J. Electroanal. Chem., 16, 285 (1968).

22. P. Delahay and V. S. Srinivasan, J. Phys. Chem., 70, 420 (1966).

23. D. J. Schiffrin, Croat. Chem. Acta, 44, 139 (1972).

24. H. Berg and H. Schweiss, Electrochim. Acta, 9, 425 (1964).

25. H. Imai and K. Yamashita, Bull. Chem. Soc. Japan, 42, 578 (1969).

26. L. I. Korshunov, Y. M. Zolotovitskii, and V. A. Benderskii, Electrokhimiya, 4, 499 (1968).

27. V. Concialini and O. Tubertini, J. Electroanal. Chem., 57, 413 (1974).

28. J. K. Sass, R. K. Sen, E. Meyer, and H. Gerischer, Surf. Sci., 44, 515 (1974).

29. A. M. Brodsky and Yu. Ya. Gurevich, Electrochim. Acta, 13, 1245 (1968).

30. H. Gerischer, E. Meyer, and J. K. Sass, Ber. Bunsenges. Physik. Chem., 76, 1191 (1972).

31. For $Ru(bipy)_3^{2+}$, photocurrents were too small to measure on the oscilloscope. Risetimes were monitored by the phase shift of the AC photocurrent signal relative to the chopped excitation beam, using the lock-in amplifier. At 10 mM, one experiment yielded phase shifts indicative of a fast risetime, but two subsequent experiments contradicted this initial result.

32. L. P. Gary, K. deGroot, and R. C. Jarnagin, J. Chem. Phys., 49, 1577 (1968).

33. J. B. Birks, J. H. Appleyard, and R. Pope, Photochem. Photobiol., 2, 493 (1963).

34. P. S. Engel and B. M. Monroe, Adv. Photochem., 8, 299 (1971).

35. C. A. Parker, "Photoluminescence of Solutions", Elsevier Publishing Co., Amsterdam, 1968, p. 315.

36. C. R. Bock, T. J. Meyer, and D. G. Whitten, J. Amer. Chem. Soc., 96, 4710 (1974).

37. C. R. Bock, T. J. Meyer, and D. G. Whitten, J. Amer. Chem. Soc., 97, 2909 (1975).

PART II: The Mechanism of Dye-Sensitized Photocurrents at a Tin-Oxide Electrode

INTRODUCTION

In Part I, it was concluded that observation of net charge transfer between photoexcited molecule and a metal electrode was improbable because of the high quenching efficiency of the metal. Calculations and measurements by Kuhn [1] and others [2, 3] have shown that luminescence lifetime rapidly drops to zero at distances closer than 100 Å to a metal surface because of energy transfer from the emitter to the metal. Even if charge transfer did occur, the reverse exchange could easily return the molecule to its ground state with no net photocurrent [4] (Fig. II-1). By contrast, the presence of a band gap, a region devoid of energy levels, in a semiconductor prevents either mechanism from suppressing the photocurrent. If the band gap is greater than the excitation energy of the molecule, energy transfer cannot occur because a corresponding transition cannot be excited in the semiconductor. Under the same condition only one of the molecular energy levels can overlap with a semiconductor energy level; the reverse electron exchange is prevented. Excitation with photon energies less than the band gap has the further advantage that the

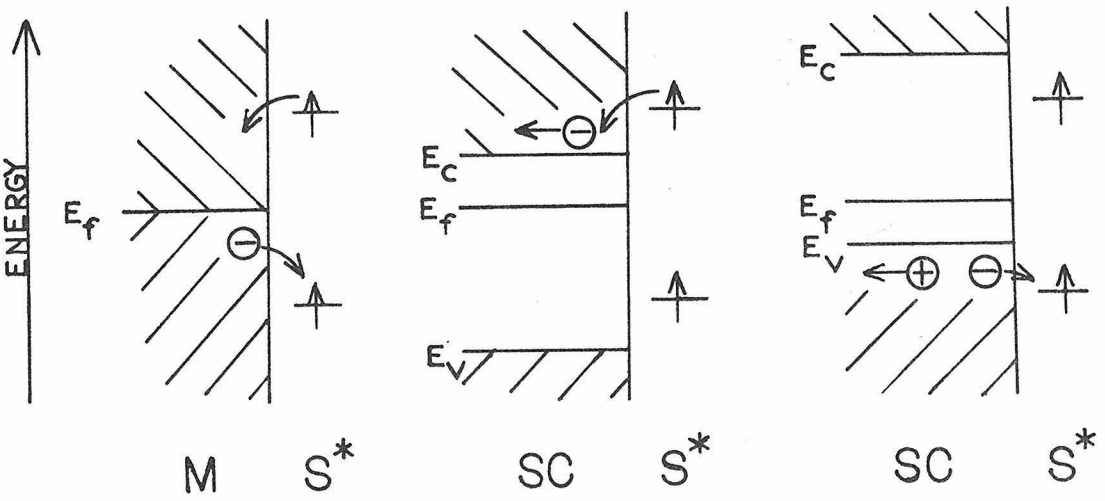

Fig. II-1. Energy Level Diagram and Mechanism for Sensitization Processes on Metals and Semiconductors

M -- metal; SC -- semiconductor; S^* -- excited sensitizing molecule; E_f -- Fermi level; E_v -- valence band; E_c -- conduction band.

semiconductor is reasonably transparent at those wavelengths, permitting excitation of the dye with a beam passing through the electrode. Work by Gerischer, Memming, Tributsch, and Hauffe [4-14] have indeed shown electron transfer between a photoexcited dye and a semiconductor electrode. The basic experimental apparatus consisted

of a single crystal of a wide band-gap semiconductor, typically ZnO or GaP, functioning as the working electrode in a standard three-electrode electrochemical cell containing electrolyte plus dye.

Gerischer et al. considered adsorption of the dye onto the surface of the semiconductor to be necessary for charge transfer to occur during the lifetime of the excited dye. Considerable experimental evidence has been obtained for photocurrents originating from adsorbed layers. Dye layers irreversibly adsorbed onto semiconductors via the Langmuir-Blodgett technique produce sensitized photocurrents [4,15]; the photocurrents rapidly decayed with time, indicating consumption of the dye. Memming and Tributsch [9] reported seeing the dimer absorption band of methylene blue and polymer absorption band of pseudoisocyanine in the sensitization spectra (photocurrent dependence on exciting wavelength) at solution concentrations too low for the observation of these same bands in solution absorption spectra. They proposed surface-induced aggregation of the dyes. A unique double-dye competition experiment by Memming [10] utilized the tendency for methylene blue to displace eosin on a surface. A sensitization spectra was obtained with eosin in the solution. Upon addition of methylene blue, the eosin peak dropped immediately, and the methylene blue peak slowly appeared, requiring 30 min to reach a maximum. The initial sharp drop of the eosin peak was attributed

to energy transfer to the lower energy excited states of the methylene blue molecules not yet adsorbed to the electrode.

An obvious variable in adsorption studies is the concentration. The dependence of the sensitized photocurrent upon the concentration of the dye rhodamine B has been measured in three separate laboratories, with slightly different results each time. Tributsch and Gerischer [7] found that the sensitized photocurrent was roughly proportional to concentration below ca. 10^{-4} molar; however, saturation was reached at 10^{-3} molar. Hauffe et al. [12] also observed linear concentration dependence at low concentrations, and decreasing slope with increasing concentration, but even at 10^{-3} M, no plateau was evident. Both experiments were performed in aqueous solution on single crystals of ZnO. Finally, Kim and Laitinen [16] observed a vaguely sigmoidal concentration dependence (no background photocurrent correction) on polycrystalline SnO_2 electrodes, but the "plateau" occurred at ca. 10^{-5} M. These results do not permit easy interpretation due to several complicating factors. First, aqueous rhodamine B solutions contain significant concentrations of dimers above 10^{-4} M, and at 10^{-3} M, roughly equal amounts of monomer and dimer are present. The dimer absorption peak, which occurs at higher energies, has been found in the sensitization spectra [12], but the sensitization factor appeared to be less for the dimer than for the

monomer. One possible interpretation is that only the excited monomer transfers an electron to the electrode, and the photoexcited dimer transfers its energy to the monomer with less than 100% efficiency. In any case, a graph of photocurrent versus total dye concentration above 10^{-4} M levels does not accurately reflect the true concentration dependence. The second factor relates to the apparent irreversibility of the adsorption process. Using C-14 labeled rhodamine B, Laitinen found that a monolayer was rapidly formed on SnO_2, and that washing with water did not disturb it [16]. Consistent with this behavior is the evidence of chemisorption obtained with fluorescence excitation and emission spectra [17]; Hauffe and Bode concluded that rhodamine B forms a zinc carboxylate on the ZnO surface through reaction with surface hydroxyl groups (Fig. II-2). The benzoic acid substituent is oriented perpendicular to the plane of the xanthene moiety and is not part of the chromophore [18]. Many of

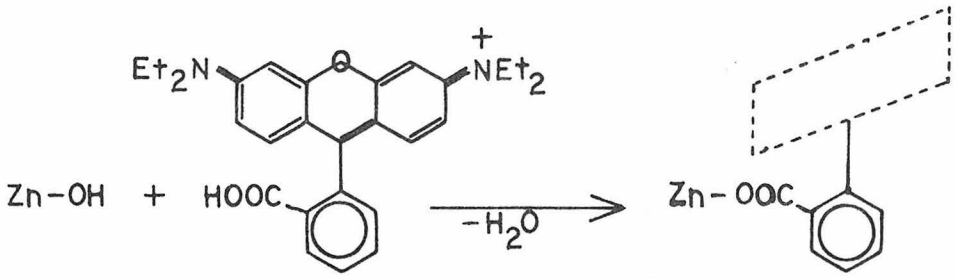

Fig. II-2. Reaction of Rhodamine B with a Surface Hydroxide

the dyes commonly used in sensitization experiments contain the benzoic acid substituent and are susceptible to the same reaction (Fig. II-3), so further studies of the concentration dependence seem worthwhile.

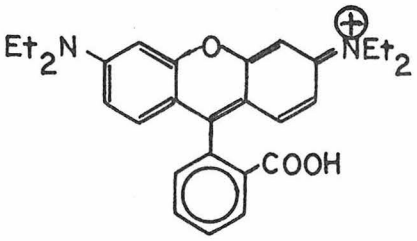

Rhodamine B

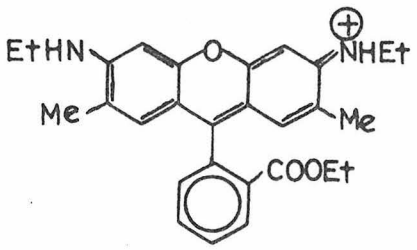

Rhodamine 6G

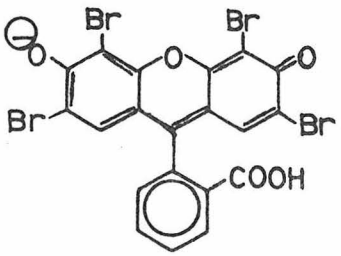

Eosin

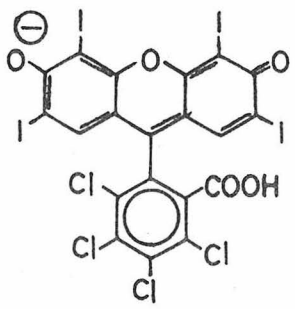

Rose bengale

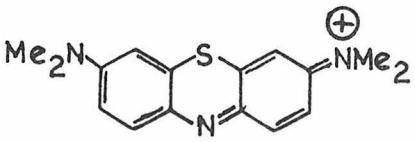

Methylene blue

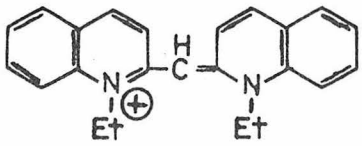

Pseudoisocyanine

Fig. II-3. Common Sensitizing Dyes

All of the above experiments were conducted in aqueous solutions. In water, all of the dyes in Fig. II-3 form dimers or higher aggregates at moderate concentrations ca. 10^{-4} M or higher. Hydrophobic forces are the primary cause of aggregation[18], despite the coulombic repulsion that must exist in these ionic dyes. In alcohols and other organic solvents, monomer absorption spectra are obtained at even the highest possible concentrations. Hence, a concentration dependence study in a nonaqueous solvent would clarify the role of the monomer both in adsorption and in the sensitization mechanism. It has been shown[19] that aggregates, or micelles, of cationic dyes adsorb onto an anionic hydrated SiO_2 surface via coulombic attraction, giving surface concentrations well in excess of that expected for a monolayer. Assuming that the same type of interaction exists on a SnO_2 surface, one would predict the adsorption of isolated molecules from a nonaqueous solvent, and aggregates from aqueous solutions. Only one study of dye sensitization in a nonaqueous solvent has been reported[12]. Hauffe et al. found that as the concentration of rhodamine B in methanol increased, the photocurrent at a ZnO electrode saturated at concentrations above 2×10^{-4} M. However, this result did not agree with adsorption isotherms obtained on ZnO powder, where no saturation of adsorbed dye concentration was observed.

An important question concerning the mechanism of sensitization is from which excited state, the singlet or the triplet state, does the actual charge transfer take place? The only definite assertion on this question has been made by Memming[15]. His experiment entailed adsorbing stearyl derivatives of oxacarbocyanine dyes diluted with arachidic acid onto polycrystalline SnO_2, and comparing sensitized photocurrent spectra with absorption, fluorescence, and phophorescence spectra. The quantum yield of the photocurrent decreased with increasing concentration while absorption spectra revealed with formation of dimers and higher aggregates, so polymers were not involved. The intensity of the phosphorescence was nearly independent of dye concentration, so Memming concluded that the triplet state was not involved in the charge-transfer process, leaving only the lowest excited singlet state of the monomer. Other evidence contradicts this conclusion. In Memming's experiments, and other experiments[4, 5, 7, 14], certain chemical agents known as supersensitizers are found to greatly increase the dye-sensitized photocurrents. The general hypothesis has been that the supersensitizers react with the excited dye prior to charge transfer[4, 7, 10, 14, 20], e.g., a reducing agent reduces the excited dye, which then injects an electron into the semiconductor. But a prior bimolecular reaction favors the much longer-lived triplet state. Secondly, many of the dyes used as sensitizers contain heavy

atoms which enhance intersystem crossing to the triplet state[18]; see, for example, the dyes rose bengale, eosin, and methylene blue in Fig. II-3. High triplets yields for methylene blue and eosin have been observed[18].

The dye we chose for the experiments was the well-known laser dye, rhodamine 6G (henceforth abbreviated RH6G); see Fig. II-3. RH6G is one of the more photochemically stable laser dyes, and has a very low triplet yield ($\phi_t \leq .01$)[18]. Its chief advantage over rhodamine B is the presence of the ethyl ester rather than the free acid. The ester group prevents the formation of a lactone, with destruction of the chromophore, in basic solvents, as is shown for rhodamine B in Fig. II-4. It also should inhibit the chemisorption reaction shown in Fig. II-2.

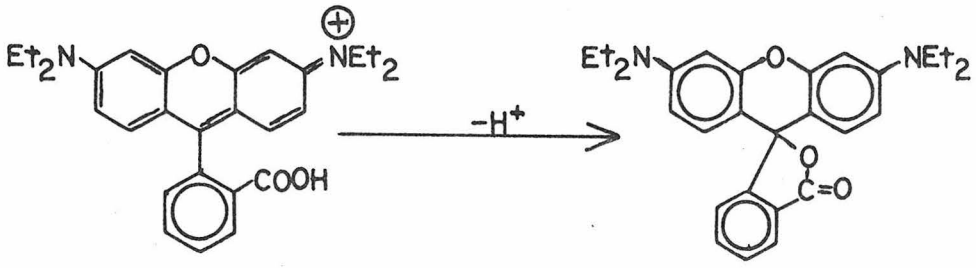

Fig. II-4. Lactone Formation of Rhodamine B

EXPERIMENTAL

Semiconductor electrode

All experiments were performed with homemade polycrystalline tin-oxide electrodes. The electrical and optical bulk properties of polycrystalline SnO_2 have been investigated[21, 22]. The material is an n-type semiconductor with typical carrier densities of $10^{19}/cm^3$. The high doping level has been attributed to oxygen deficiency and residual chloride impurity. Crystallinity has been proven by sharp x-ray diffraction patterns.

The polycrystalline electrodes were made by spraying an acidic Sn(IV) solution in an oxygen stream onto a hot (500°C) substrate. Two spraying mixtures were tried without any significant change in the properties of the electrodes. The first contained 50 ml of glacial acetic acid, 15 ml of concentrated hydrochloric acid, and 20 ml of $SnCl_4$; the second contained 50 ml of glacial acetic acid mixed with 20 ml of $(C_4H_9)_3SnCl$. Best results were obtained when the substrate was rotated 90° and allowed to reheat between each spraying. The first substrates were quartz slides. Problems with high internal resistance led to the use of the double coating technique suggested by Kim and Laitinen[16], in which the substrate was a commercially purchased highly doped SnO_2 layer deposited on Pyrex. Thickness of the

deposited layers was measured by monitoring the interference fringes in the electrode absorption spectrum (Fig. I-5). Thickness was calculated by the relation $t = (2n\Delta\bar{\nu})^{-1}$, where n is the refractive index (= 2.0 [21]), and $\Delta\bar{\nu}$ is the distance between successive maxima in wavenumbers. Typical thicknesses were 0.3-0.6 microns. Ohmic contacts were provided by painting the SnO_2 surface with silver conducting paint. No rectification of current was observed between separated silver paint patches.

Measurement of the carrier concentration and flat band potential followed the procedure outlined by Mollers and Memming [23]. To measure the space charge capacitance, a sinusoidal potential was applied to the electrochemical cell and the magnitude and phase shift of the current measured with an Ithaco 391A lock-in amplifier.

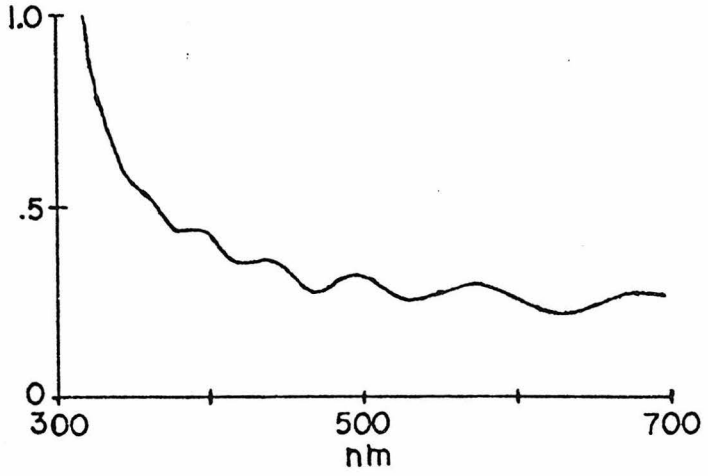

Fig. I-5. SnO_2 OTE Absorption Spectrum

Photoelectrochemical cells

Two electrochemical cells were employed for photocurrent measurements. In both cells, the working electrode area was 0.20 cm^2. The first cell, described in Part I (Fig. I-3; cell #2), was vacuum-tight; the electrode was epoxied onto the cell with TORR-SEAL. The cell's main advantages were the achievement of high solvent purity and extremely low oxygen concentrations. The primary disadvantages were threefold: one did not know the reference electrode potential until the end of the experiment; only one addition of dye to the solution was possible; and the cell had to be removed from the optical train in order to add the dye.

The second cell (Fig. I-6) was designed especially for concentration dependence experiments. Aliquots of dye solution were added through the top, the solution mixed by the action of the bubbler, and a sample removed via the stopcock for spectroscopic determination of the concentration. The SnO_2 electrode was clamped by spring pressure onto the flat ground face covered with a 0.005 inch thick Teflon washer; detail is shown in Fig. II-6.

Solvent/supporting electrolyte systems were 0.2 M NaF in water adjusted to pH 7, and 0.1 M tetraethylammonium perchlorate (TEAP) in acetonitrile. The reference electrode consisted of an Ag/Ag^+ couple in the appropriate solvent and electrolyte; potentials

Fig. II-6. Electrochemical Cell for Concentration Studies

W -- working electrode (SnO_2)
R -- reference electrode
C -- counter electrode
BP -- base plate
CP -- clamp plate
F -- flange
G -- flat ground surface
TW -- teflon washer
S -- spring

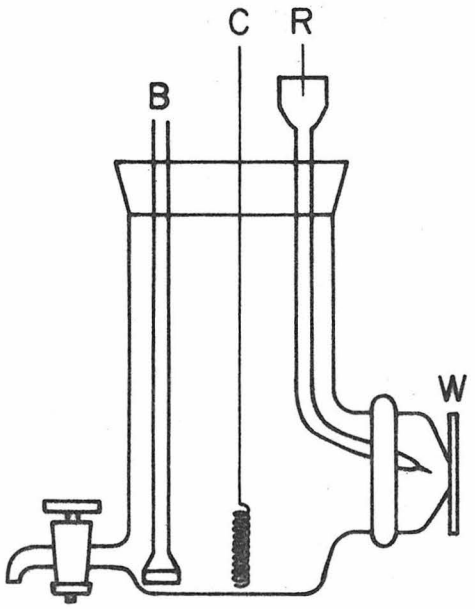
C
R
B
W

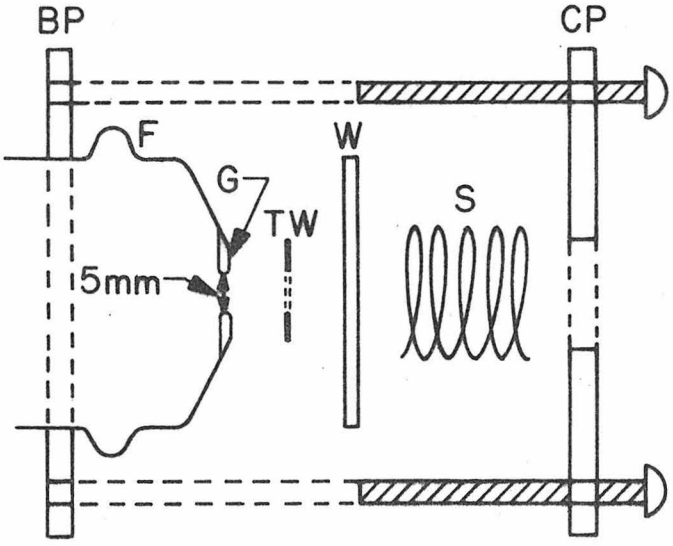
BP
CP
F
W
G
TW
S
5mm

were checked against an NaCl saturated calomel electrode before and after each experiment. A deoxygenated stream of argon saturated with solvent was bubbled continuously through the solution, providing continuous stirring.

Photocurrent measurement technique

The experimental techniques have been described in Part I. Most of the measurements were made with the Ithaco 391A lock-in amplifier and PAR variable speed light chopper. Optimal operating frequency appeared to be 20-25 Hz. Lower frequencies required longer instrumental response times, and at higher frequencies (> 60 Hz), the cell and potentiostat started to pick up noise from the light chopper, despite the Faraday cage. Maximum photocurrent sensitivities of ± 0.05 nA were attainable.

Monomer-dimer equilibria

Laser grade rhodamine 6G was purchased from Matheson, Coleman, and Bell, and used without further purification. Despite the undesirability of chloride (it limits the oxidative potential range) as a counter ion, the dye was not converted to the perchlorate salt because of its low solubility in water. The monomer has a molar extinction coefficient of 92,000 at 526 mμ in both water and acetonitrile. Figure II-7 demonstrates the absorption change observed with dimer

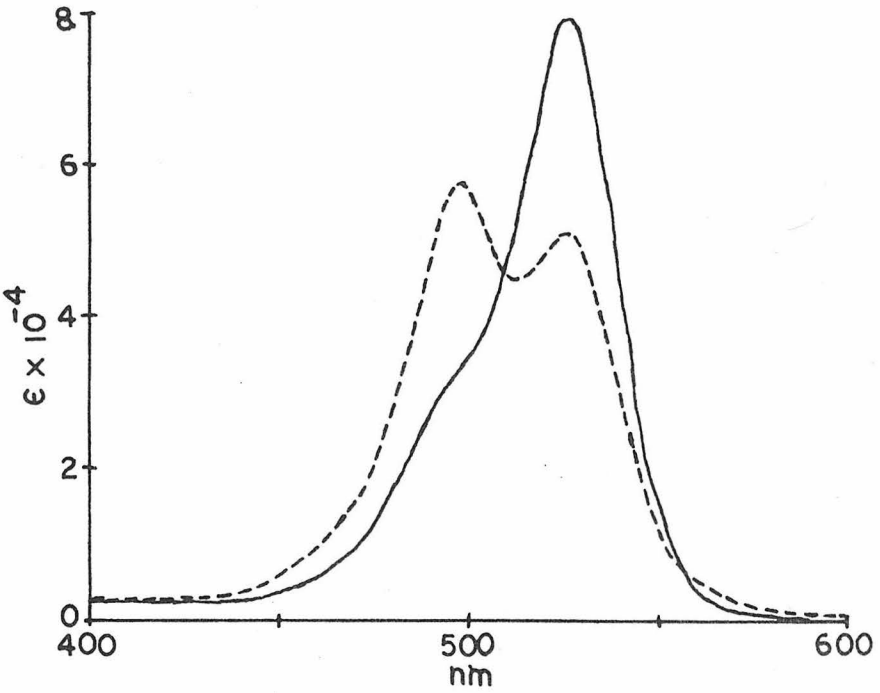

Fig. II-7. Rhodamine 6G Absorption Spectrum in H_2O

——— 6×10^{-6} M

- - - - 6×10^{-4} M

formation. The equilibrium constant and molar extinction coefficients for the monomer and dimer at 526 mμ were calculated from absorption data at three different total concentrations and the following equations:

$$M + 2D = C$$

$$K = \frac{D}{M^2}$$

$$A = \epsilon_M M + \epsilon_D D$$

M = monomer concentration
D = dimer concentration
C = total concentration
K = equilibrium constant
A = optical absorption

From these equations, the following useful relations may be derived.

$$M = \frac{1}{4K}\left(\sqrt{8KC + 1} - 1\right)$$ (monomer concentration from total concentration)

$$M = \frac{1}{2K\epsilon_D}\left(\sqrt{\epsilon_M^2 + 4K\epsilon_D A} - \epsilon_M\right)$$

$$C = M + 2K M^2$$

(monomer and total concentration from absorbance)

For RH6G in water, K = 3900 liters/mole, ϵ_M = 92,000, and ϵ_D = 27,000 liters/mole/cm.

Fluorescence quenching

A small electrochemical cell was constructed to fit in the sample compartment of a Perkin-Elmer MPF-3 Fluorescence Spectrophotometer (Fig. II-8). To maximize fluorescence emission from an adsorbed dye later relative to solution species, excitation was accomplished by total internal reflection (TIR)[24, 25] of the excitation beam at the electrode-solution interface (Fig. II-9).

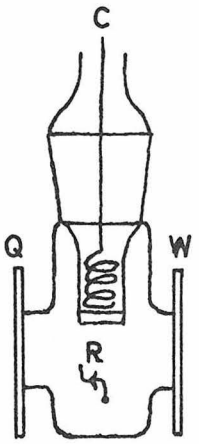

Fig. II-8. TIR Cell

W -- SnO_2 working electrode
R -- reference electrode
C -- counter electrode
Q -- quartz window

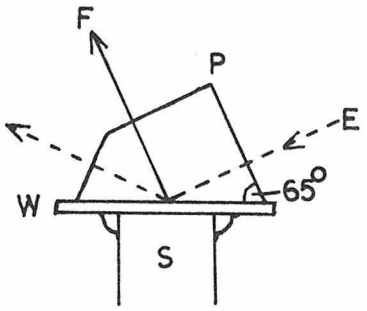

Fig. II-9. TIR Geometry-Top View

W -- SnO_2 working electrode
S -- supporting electrolyte and dye
P -- quartz prism
E -- excitation beam
F -- fluorescence towards emission monochromator

A special quartz prism provided perpendicular faces for the incident and reflected excitation beam, and a third face perpendicular to fluorescence directed towards the emission monochromator slit. The prism was optically coupled to the electrode (quartz substrate) by a thin layer of glycerin (index of refraction = 1.46 for both quartz and glycerin), which also provided the necessary adhesion forces to hold the prism on. The cell also had a quartz window for comparison of fluorescence behavior in the absence of the SnO_2 layer.

RESULTS AND DISCUSSION

Excellent treatments of semiconductor properties and their effects in electrochemistry have already been published[26-28]. A brief treatment is presented below to facilitate later discussion.

Materials having semiconducting properties are characterized by the presence of two energy bands separated by a band gap[29]. The lower energy band is called the valence band, and is nearly filled with electrons; the higher energy band, or conduction band, is nearly empty. Excitation of an electron from the lower band to the upper band produces two potential current carriers, the electron in the conduction band and the hole, or vacant orbital, in the valence band. In a wide band-gap semiconductor, room temperature thermal excitation produces such a low concentration of current carriers that the material is essentially an insulator. Introduction of impurities into the crystalline lattice can produce donor and acceptor levels within the band gap but close to the conduction and valence bands, respectively. For an n-type semiconductor, donor level densities predominate, and thermal ionization results in a large increase in the mobile electron concentration. Charge carrier densities can be modulated over many orders of magnitude by controlling the type and concentration of impurities; typical values range from 10^{13} to 10^{19}

carriers/cm^3.

Consider a semiconductor placed in contact with a concentrated electrolyte. The charge carrier density in 0.1 M 1:1 electrolyte is roughly $10^{20}/cm^3$, considerably higher than in the semiconductor. As a result, when an external potential is applied, i.e., when the semiconductor electrode potential is changed with respect to a reference electrode in contact with the electrolyte, most of the potential drop occurs within the semiconductor. The energy of the bands within the bulk increases or decreases linearly with applied potential; a more positive potential lowers the energy of the bands. However, these bands remain at constant energy at the interface, so that near the interface, the energy of the bands must change. The extent and direction of the band-bending can be controlled by applied potential. Figure II-10 demonstrates this process. The potential gradient also redistributes the charge carrier density near the interface, producing the so-called space charge layer. At a certain potential known as the flat-band potential, charge carrier density is uniform throughout the semiconductor. In any region where there is a potential and charge carrier gradient, there exists a differential capacitance $\frac{dQ}{dV}$. Hence, across the semiconductor-electrolyte interface there are now three capacitances: the space charge capacitance within the semiconductor, the inner layer, or Helmholtz capacitance for the region between the

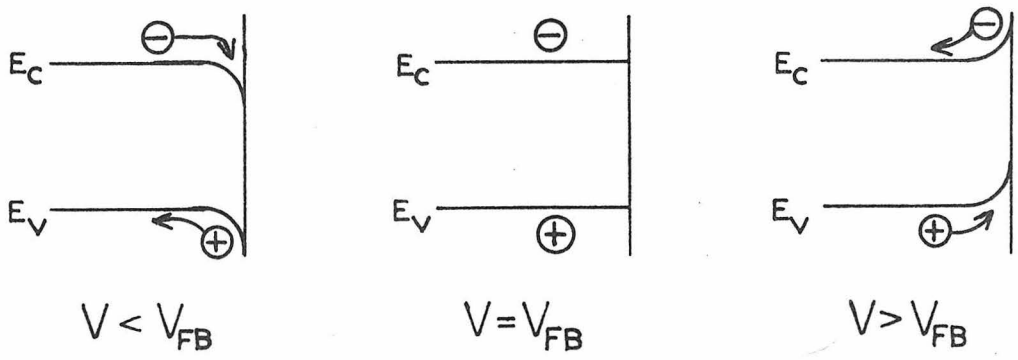

Fig. 10. Band-Bending as a Function of Potential

E_c = bottom of the conduction band; E_v = upper edge of the valence band; V = applied potential. V_{FB} = flat-band potential. On this and subsequent figures of this type, the vertical axis represents increasing energy, and the horizontal axis distance from the solution interface within the semiconductor.

electrode surface and the plane of closest approach of solvated ions, and the diffuse layer capacitance (Fig. II-11). The capacitances are in series, so that the smallest capacitance dominates the cell impedance. A high electrolyte concentration (such that $\sigma_{solution} > \sigma_{semiconductor}$) makes V_D and consequently $\frac{1}{C_D}$ negligibly small. Hence, variations in the applied potential lead mainly to changes in ΔV_{SC}, the potential drop across the space charge layer [23, 30-32], i.e., $\Delta V_{SC} = V - V_{FB}$. When an n-type semiconductor is biased

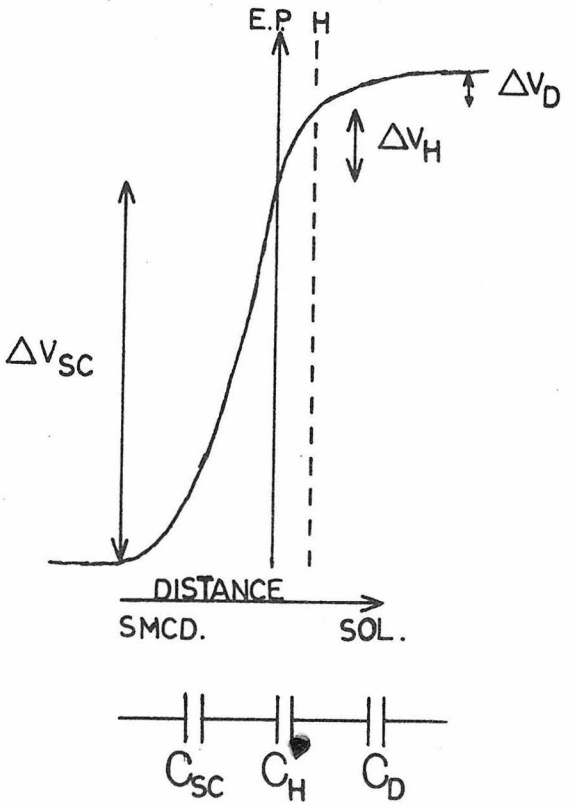

E.P. -- electrical potential
SC -- space charge layer
H -- Helmholtz plane
D -- diffuse layer

$$\frac{1}{C} = \frac{1}{C_{SC}} + \frac{1}{C_H} + \frac{1}{C_D}$$

Fig. II-11. Potential Gradient and Capacitances for a Semiconductor-Electrolyte Interface

positive of the flat-band potential, electrons, the majority carriers, are depleted from the surface. Under such conditions, the space charge capacitance is given by the Schottky-Mott equation:

$$C_{SC} = \left(\frac{\epsilon \epsilon_0 e\, n_0}{2}\right)^{1/2} \left(\Delta V_{SC} - \frac{kT}{e}\right)^{1/2}$$

ϵ and ϵ_0 are the dielectric constants of SnO_2 and vacuum, respectively, e the electron charge, n_0 the carrier concentration, and $\frac{kT}{e}$ the electron volt equivalent of thermal energy. This may be rearranged to obtain

$$\frac{1}{C_{SC}^2} = \left(\frac{2}{\epsilon \epsilon_0 e\, n_0}\right)\left(V - V_{FB} - \frac{kT}{e}\right)$$

$$\frac{kT}{e} = .025 \text{ eV at } 25^\circ C; \quad \epsilon_{SnO_2} = 10$$

Thus, a plot of the reciprocal square of the experimental capacities versus the potential should yield a straight line with intercept $V_{FB} + \frac{kT}{e}$ and slope inversely proportional to carrier concentration.

$$n_0 = \frac{1}{\epsilon \epsilon_0 e} \frac{dV}{d(1/C^2)}$$

Figure II-12 shows the results obtained for different electrodes in water and acetonitrile using the vacuum-tight cell. For all of the double-coated electrodes, n_0 was found to be $2.0\ (\pm.5) \times 10^{19}/cm^3$. A Hall effect measurement was attempted on a single-coated electrode to provide a separate value of the carrier concentration. The attempt failed because the thin ($0.5\ \mu$) tin-oxide layer had too high a resistance; the current densities necessary for measurable Hall effect voltages could only be obtained with disastrously high supply voltages.

Fig. II-12. Plot of $\frac{1}{C^2}$ vs. Applied Potential

Measuring frequency 1000 Hz; two separate double-coated electrodes.

⊙ -- 0.2 M NaF/H_2O, $n_0 = 1.8 \times 10^{19}/cm^3$

△ -- 0.1 M $TEAP/CH_3CN$, $n_0 = 2.5 \times 10^{19}/cm^3$

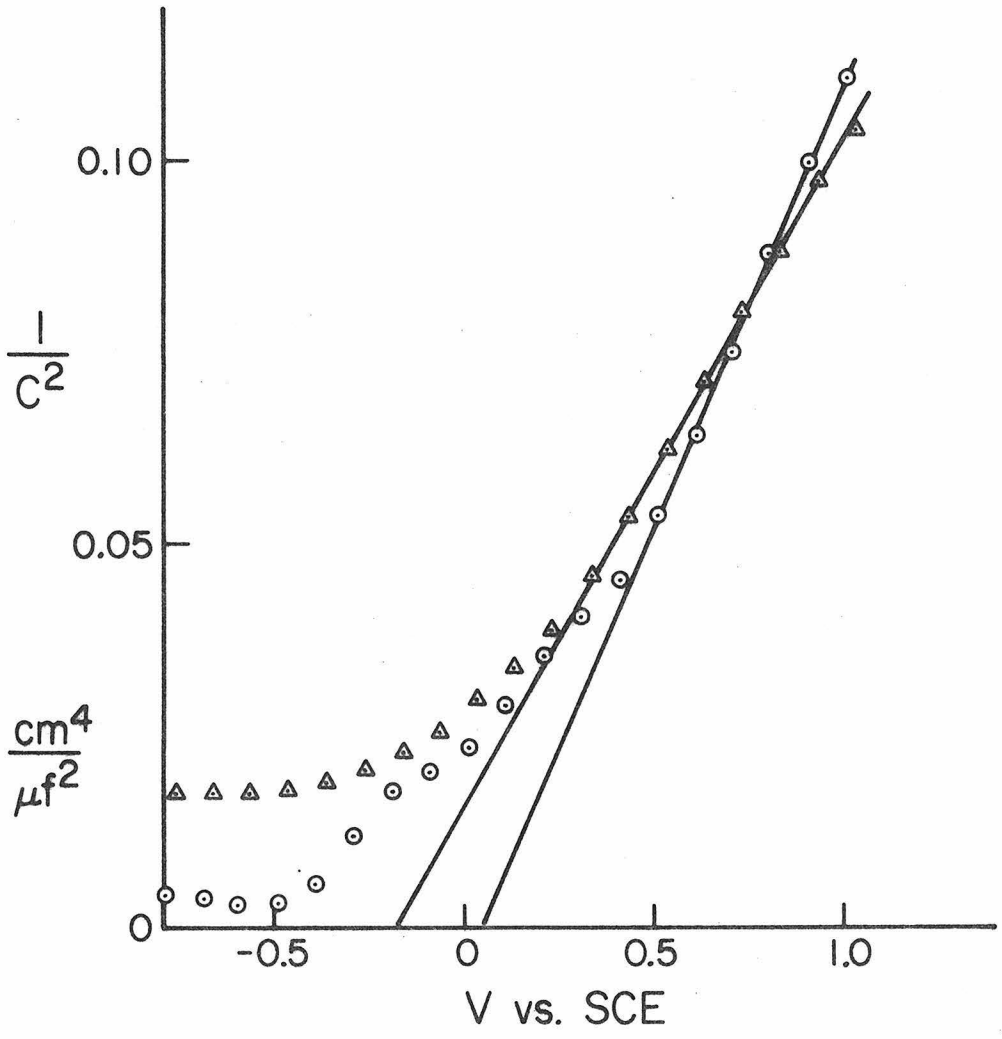
0.10
0.05
0
$\frac{1}{C^2}$
$\frac{cm^4}{\mu f^2}$
-0.5
0
0.5
1.0
V vs. SCE

Values for V_{FB} were less reliable; intercepts varied between 0 and +0.3 V vs. SCE, even for the same electrode in separate experiments. Addition of RH6G to the solution had only a small effect on V_{FB} and n_0. Frequency dispersion in the experimental capacitances was evident. Capacitances measured at 100 Hz were uniformly larger than at 1000 Hz, leading to higher calculated carrier concentrations and a more positive V_{FB}. At the more negative potentials, the curves approached a constant value as the Helmholtz capacitance became dominant.

In Fig. II-13, the potential dependence of the photocurrent is

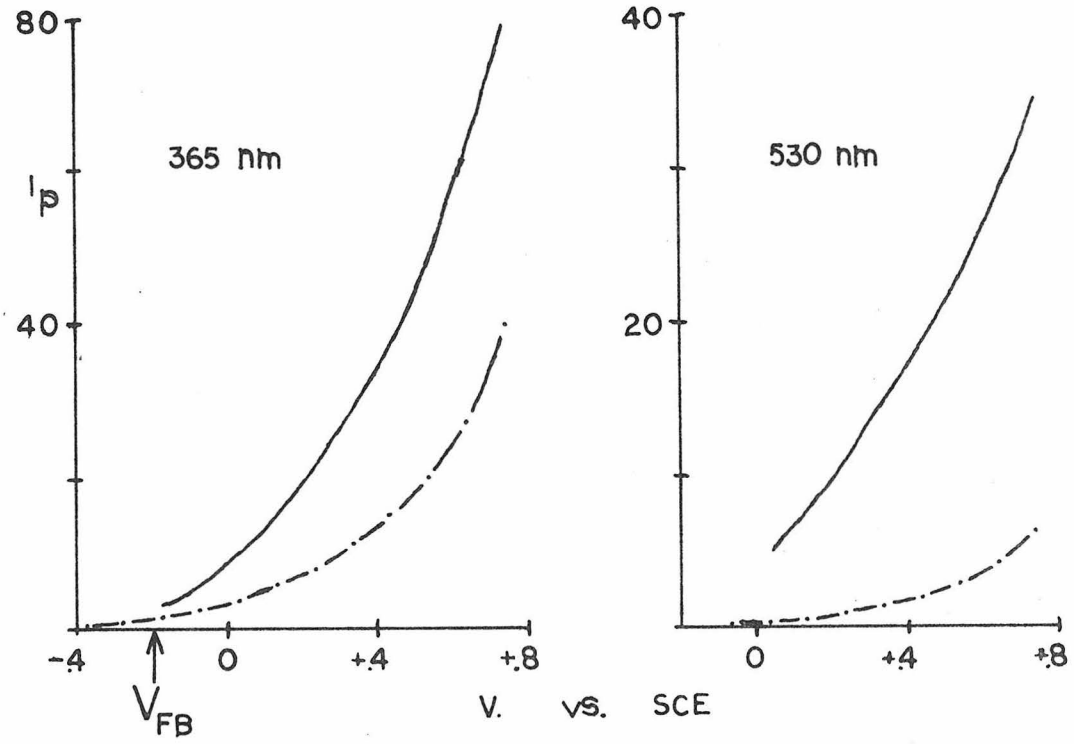

Fig. II-13. Photocurrent Potential Dependence

—·— 0.1 M TEAP/CH_3CN only, —— 1 mM RH6G

shown for two wavelengths. The general feature is a continual increase of the background photocurrent for increasing potential. Onset of the anodic photocurrents roughly coincided with the flat-band potential. At more negative potentials, and especially in the presence of dye, heating photocurrents appeared, characterized by their long rise and decay times.

The wavelength dependence of the background photocurrent is compared with the electrode absorption spectrum in Fig. II-14. Tin oxide is a wide band-gap semiconductor (3.7 eV), so strong light absorption does not occur above 350 mμ. Sizable photocurrents were obtained at much longer wavelengths. The steepness of the log i_p vs. λ curve varied for different electrodes, but appeared to be independent of solvent and monochromator slitwidth.

The mechanism of background and dye-sensitized photocurrents can now be explained in more detail. When the SnO_2 electrode is biased at a potential positive of the flat-band potential, electrons are depleted from the surface so that only holes exist at the interface, i.e., electrons from redox couples in the solution tunnel through the surface barrier to fill vacant orbitals. At constant temperature the product of the carrier density of holes and electrons is constant [29]. Therefore a high concentration of electrons, i.e., $2 \times 10^{19}/cm^3$, requires a very low hole concentration, and the current density is

Fig. II-14. Wavelength Dependence of the Background Photocurrent

Insert: Absorption spectrum of the SnO_2 electrode

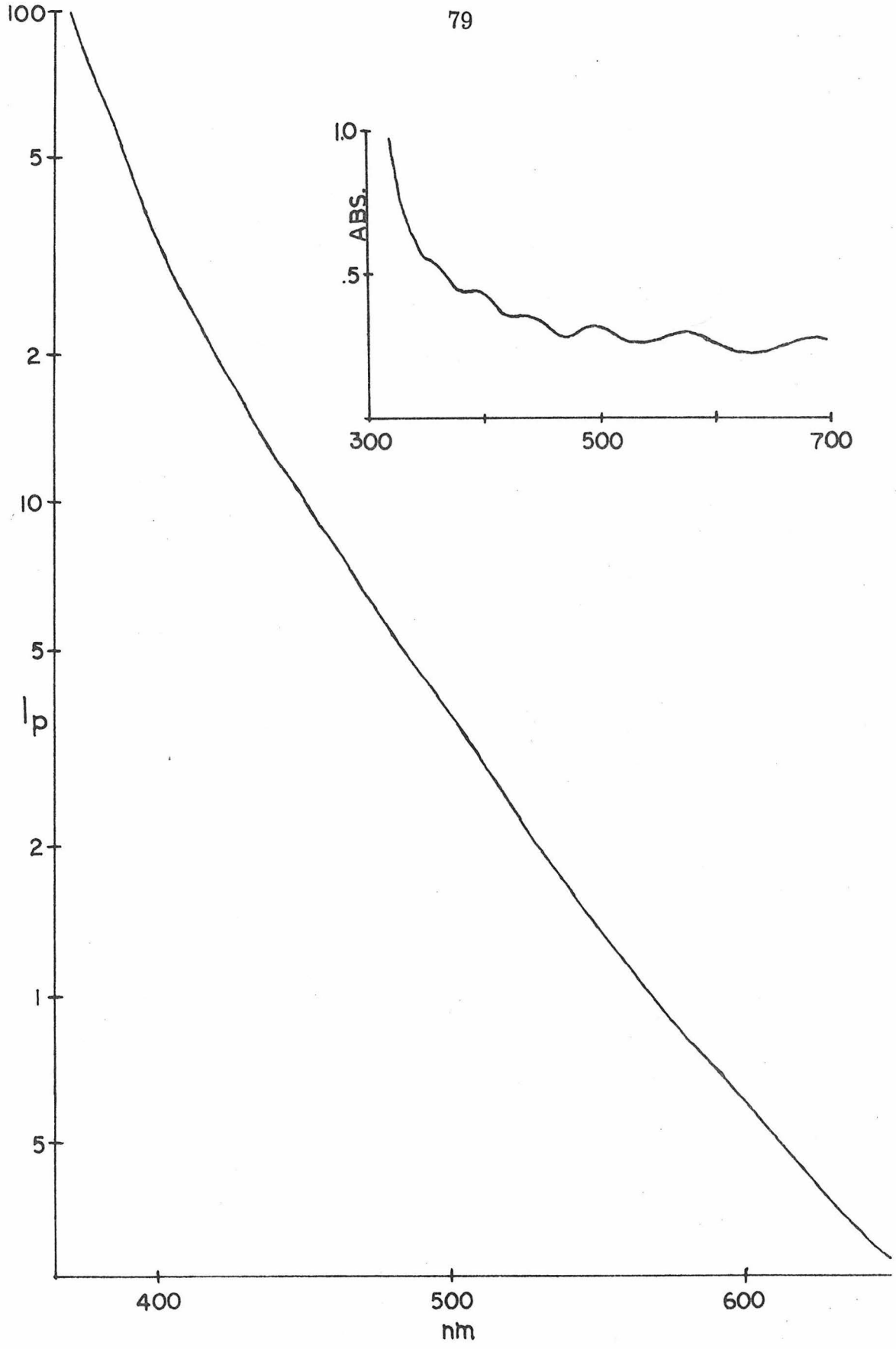
100
5
2
10
5
I_p
2
1
5
400
500
600
nm
1.0
ABS.
.5
300
500
700

limited by migration of holes to the interface. The electrode has acquired blocking character.

Illumination of the interface with photons of energy greater than the band-gap generates extra holes and electrons (Fig. II-15). Under the influence of the space charge layer, the electrons migrate towards the interior and the holes towards the surface. The sharp increase in hole surface concentration causes a photocurrent to flow. For an ideal semiconductor, in which the band gap is truly devoid of energy levels, there would be a sharp cutoff wavelength above which no photocurrent would be produced. In reality, crystal imperfections, grain boundaries, impurities, and adsorbed molecules all produce

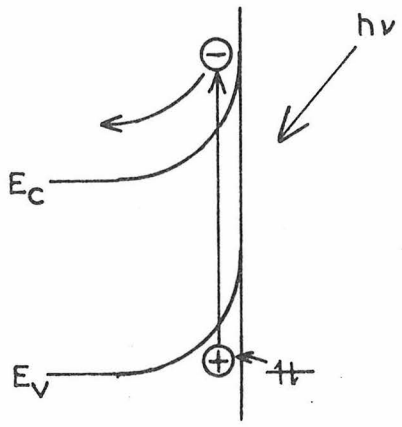

Fig. II-15. Background Photocurrent Mechanism

$$h\nu > E_c - E_v$$

intermediate energy states. These intermediate levels can produce photocurrent via the pathways shown in Fig. II-16. The high level of photocurrent obtained throughout the visible wavelengths (Fig. II-14) indicated a large number of intermediate states, as might be expected for a polycrystalline material.

The intermediate states also hasten the recombination of excess holes and electrons. In a single-crystal semiconductor electrode, the photocurrent reaches a saturation value at potentials sufficiently positive of the flat-band potential, because all of the holes photogenerated diffuse to the interface and are consumed. In contrast, no saturation of the photocurrent with increasing potential was observed at the polycrystalline SnO_2 electrodes (Fig. II-13).

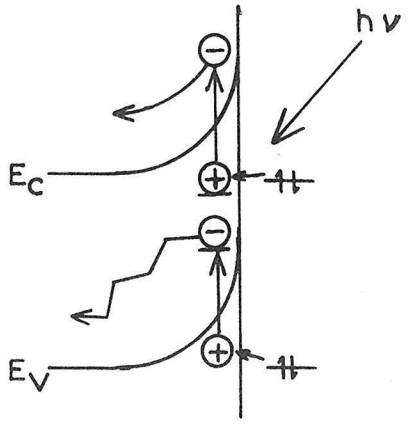

Fig. II-16. Background Photocurrent Mechanism

$$h\nu < E_c - E_v$$

The recombination rate competed sufficiently with hole diffusion so that the photocurrent never became space-charge limited[23].

The background photocurrent, and also the dye-sensitized photocurrent, exhibited pronounced time and history effects. Upon opening the mechanical shutter, the photocurrent would quickly rise to a peak value, the risetime coinciding with the natural charging time for the electrochemical cell. Then over a period of seconds the photocurrent would decay with the decay rate decreasing with time (Fig. II-17). The magnitude of the decay after a fixed time interval was most severe at high photocurrent densities (as much as 50% over ca. 1 minute), and in general appeared to be less severe in water than in acetonitrile. Allowing the cell to "rest" in the dark restored some of the initial current magnitude, especially if the solution was stirred.

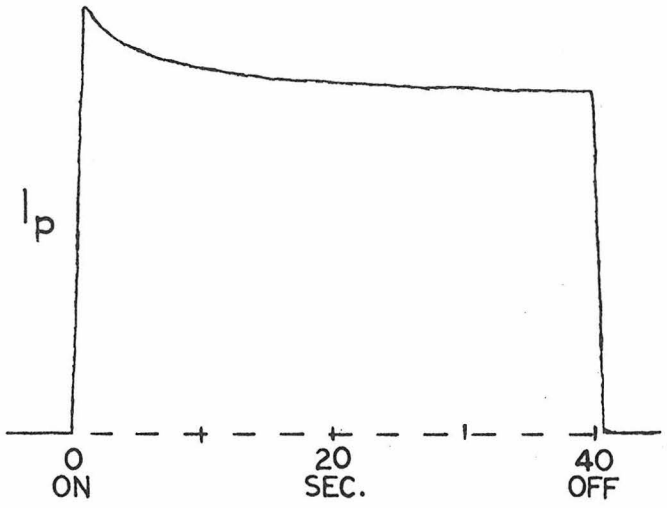

Fig. II-17. Background Photocurrent Time Decay

The decay curves were not linear with respect to $t^{-1/2}$ in unstirred solutions. The behavior suggests a slow consumption of an electroactive species with diffusion and convection from the bulk solution gradually offsetting the depletion at the surface. In aqueous solutions, the most likely candidate for oxidation by the holes is water[16]:

$$H_2O + 2h^+ \longrightarrow \tfrac{1}{2}O_2 + 2H^+$$

The presence of a time decay in water, where the bulk concentration is 55 M might imply the presence of an activated adsorbed layer as the electroactive species. Because of the general agreement on the presence of surface hydroxyl groups[16, 23] a layer of hydrogen-bonded water molecules, even in acetonitrile, must exist. A slow conversion of a hydrogen-bonded water molecule to an activated molecule prior to oxidation by a hole is then necessary to account for the time decay. The pathways to the activated species requires a high activation energy in order to explain the slow conversion.

A more viable explanation for the time decay involves the intermediate states within the space charge layer (Fig. II-16). Excess charge produced by light excitation in these states is not mobile and can accumulate, inhibiting further electron excitation. One mechanism entails the promotion of an electron from an intermediate level to the conduction band. The electron moves towards

the interior under the influence of the space charge potential gradient, preventing recombination. The photocurrent decays as neutral donor states are depleted. Suitable donor molecules at the surface can replenish the vacant levels, explaining the recovery of the photocurrent. A brief calculation demonstrates that the rate of decay is consistent with this model. Because only those intermediate states within the space charge layer will contribute to the photocurrent, it is necessary to estimate the number of states within the space charge layer, i.e., within 100 Å of the surface [23]. At wavelengths near the band-gap energy, where the background photocurrent magnitude and decay rate are maximum, excitation must be taking place from states whose densities are approaching the effective density of states at the conduction or valence band edges, e.g., $10^{19}/cm^3$ [31]. Photocurrent densities in excess of 10^{-7} A/cm^3 (10^{12} electrons/sec/cm^2) were typical at short wavelengths, so that depletion of the intermediate states would occur in 10 seconds:

$$\frac{10^{19}\ \text{states/cm}^3 \times 10^{-6}\ \text{cm}}{10^{12}\ e^-/\text{sec/cm}^2} = 10\ \text{sec}$$

Since the actual decay over tens of seconds is no more than 50%, the rate of electron replenishment must be quite rapid.

Let N be the total number of intermediate states, n the number of occupied intermediate states, and D the concentration of donor molecules. Then photocurrent is proportional to n, and

$$\frac{dn}{dt} = -k_1 n + k_2 D(N - n)$$

In water, D is assumed to be constant, and hence photocurrent decays from an initial value k_1N to the steady state value $k_1n = k_1N\left(\frac{k_2D}{k_1 + k_2D}\right)$. When the steady state photocurrent is 50% of the initial value, then $k_1 = k_2D$. Usually the magnitude of decay is not as great, so that k_2D must be larger than k_1. In acetonitrile, the magnitude of decay is larger than in water, implying that k_2D is smaller than in water. Again, the trace of water in acetonitrile could be the electron donor, with consumption of molecules at the surface now lowering D.

The second mechanism, also illustrated in Fig. II-16, involves promotion of an electron from the valence band to the vacant intermediate state. The decay rate now depends on how quickly the surplus negative charges can be removed; one can envisage a hopping process to intermediate levels further from the surface. In an n-type semiconductor, this mechanism should be relatively unimportant because the intermediate levels are occupied.

The history dependence of the photocurrent caused the most difficulty in acquiring reproducible data. The magnitude of the peak

photocurrent measured within a few seconds after opening the shutter depended on how long the solution had remained in the dark, how long the shutter had been opened on the previous measurements, whether the potential had just been changed and in which direction, and how long the cell had been held at a constant potential. Photocurrent cyclic voltammograms, obtained in the same manner as those for metal electrodes, exhibited hysteresis, i.e., anodic photocurrents at a given potential were always larger for increasing potential than for decreasing potential. Reasonably reproducible potential dependence data, as shown in Fig. II-13, could only be acquired by starting at the extreme positive potential (maximum photocurrent) and scanning to lower potential. At constant potential the general trend was a decrease in magnitude over a series of successive measurements. If the potentiostat had been turned off for a while and turned on again, or the potential had been changed to a more positive value, larger photocurrents were obtained for otherwise identical conditions. The most reproducible data for a constant potential were obtained after the electrode-electrolyte had been "conditioned" by a series of exposures to light of short wavelengths, where the highest photocurrent densities occurred. The measurement technique consisted of opening the shutter, reading the peak current on the lock-in amp. meter, closing the shutter, and waiting ca. 20-30 sec between readings. The solution

was stirred to destroy any concentration or heating gradients.

When RH6G was added to an aqueous electrolyte, an increase in photocurrent was observed at wavelengths strongly absorbed by the dye (Fig. II-18). The dye-sensitized photocurrents increased, but did not saturate with increasing potential (Fig. II-13). In contrast to the background photocurrent, dye-sensitized photocurrents involve transfer of an electron from the excited dye to the conduction band (Fig. II-19). Under the influence of the band-bending, the electron migrates towards the interior of the semiconductor, preventing the reverse electron transfer. A polycrystalline electrode would be expected to have a much lower sensitization factor than a single crystal because the higher densities of intermediate and surface states would increase the probability of reverse electron transfer. For example, the electron could leap from the excited energy level to the surface state, and then to the ground state level.

In water and acetonitrile, the wavelength of maximum sensitization varied from 520 to 540 mμ. The uncertainty arose from the large bandpass of the excitation light (33 mμ) or decreased signal-to-noise at a smaller bandpass (7 mμ). Because the solution dimer absorption peak is at 500 mμ (Fig. II-7), this species did not appear to sensitize the semiconductor, in contrast to the results obtained by Hauffe et al.[12]. The peak sensitization wavelength is reasonable for

Fig. II-18. Dye-Sensitized Photocurrent Spectrum

RH6G in H_2O

—— 0.2 M NaF/H_2O only

- - - 1.1×10^{-3} M RH6G

+.94 V vs. SCE. Log ϵ plot for RH6G monomer also shown for comparison.

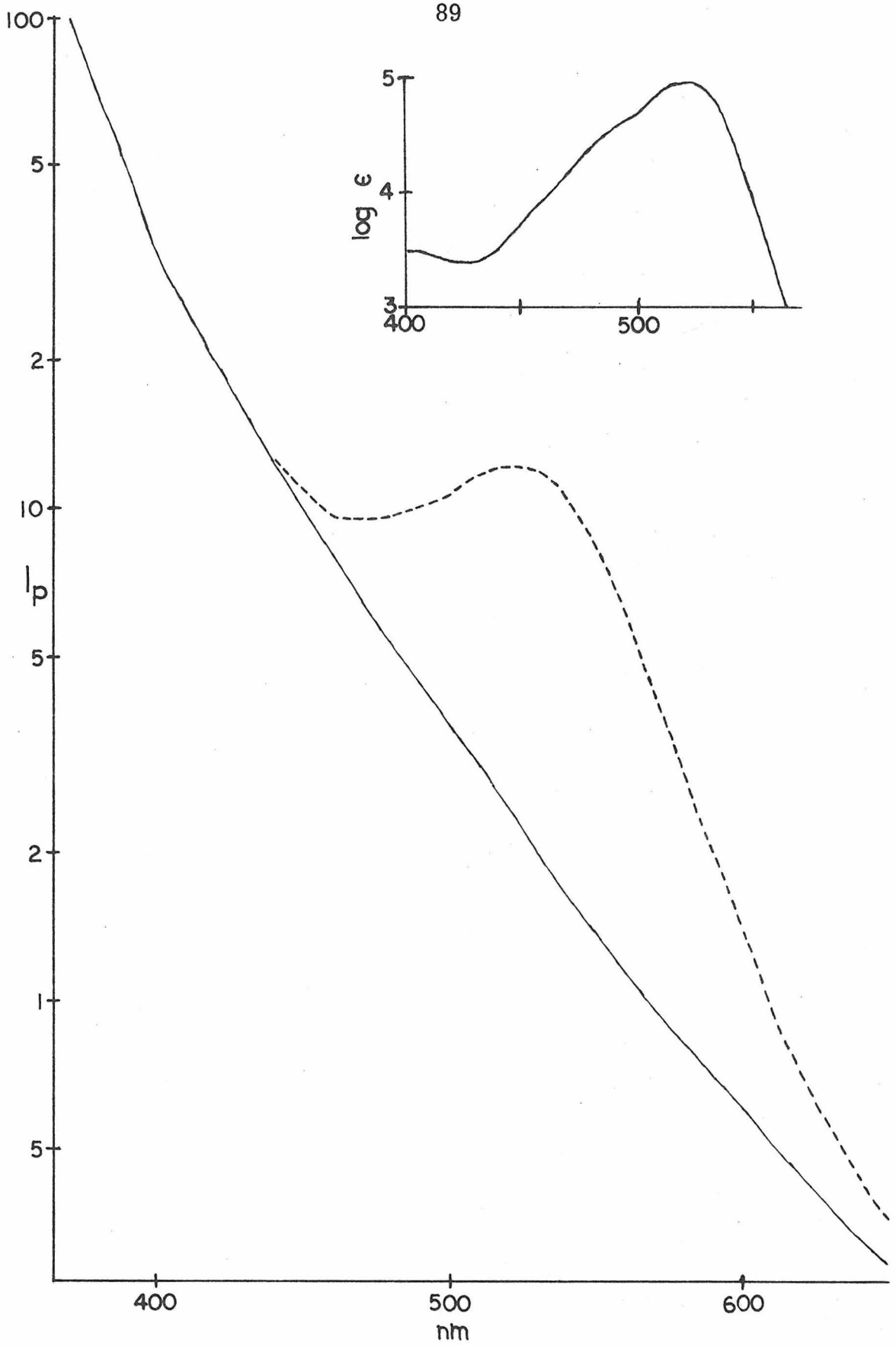
100
5
2
10
I_p
5
2
1
5
400
500
600
nm
log ε
5
4
3
400
500

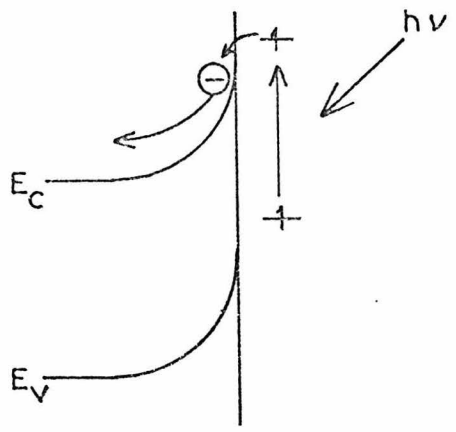

Fig. II-19. Dye-Sensitized Photocurrent Mechanism

monomer sensitization, especially if adsorption causes a slight red shift in the monomer absorption peak (526 mμ). In water, however, there is an additional complication due to the formation of a permanent adsorbed dye layer. Cationic dyes are known to form water-insoluble stains on glass[19]. Indeed, absorption spectra of RH6G layers can be obtained merely by soaking a suitable substrate in an aqueous RH6G solution, rinsing it with water, and using the 0.1 slidewire on the spectrophotometer. Figure II-20 contains the results for a polished quartz and a commerical SnO_2 surface; for comparison, the spectrum of the monomer and of a Nujol mull are included. Exactly the same spectrum appeared on both surfaces, with the absorption maximum red shifted to 545 mμ. Assuming the ϵ_{max} to be 5×10^4 liters/mole/

Fig. II-20. Spectra of Adsorbed RH6G Layers

A -- monomer in solution (10^{-5} M)

B -- layer on polished quartz (two surfaces)

C -- layer on SnO_2 OTE (one surface)

D -- Nujol mull of the solid

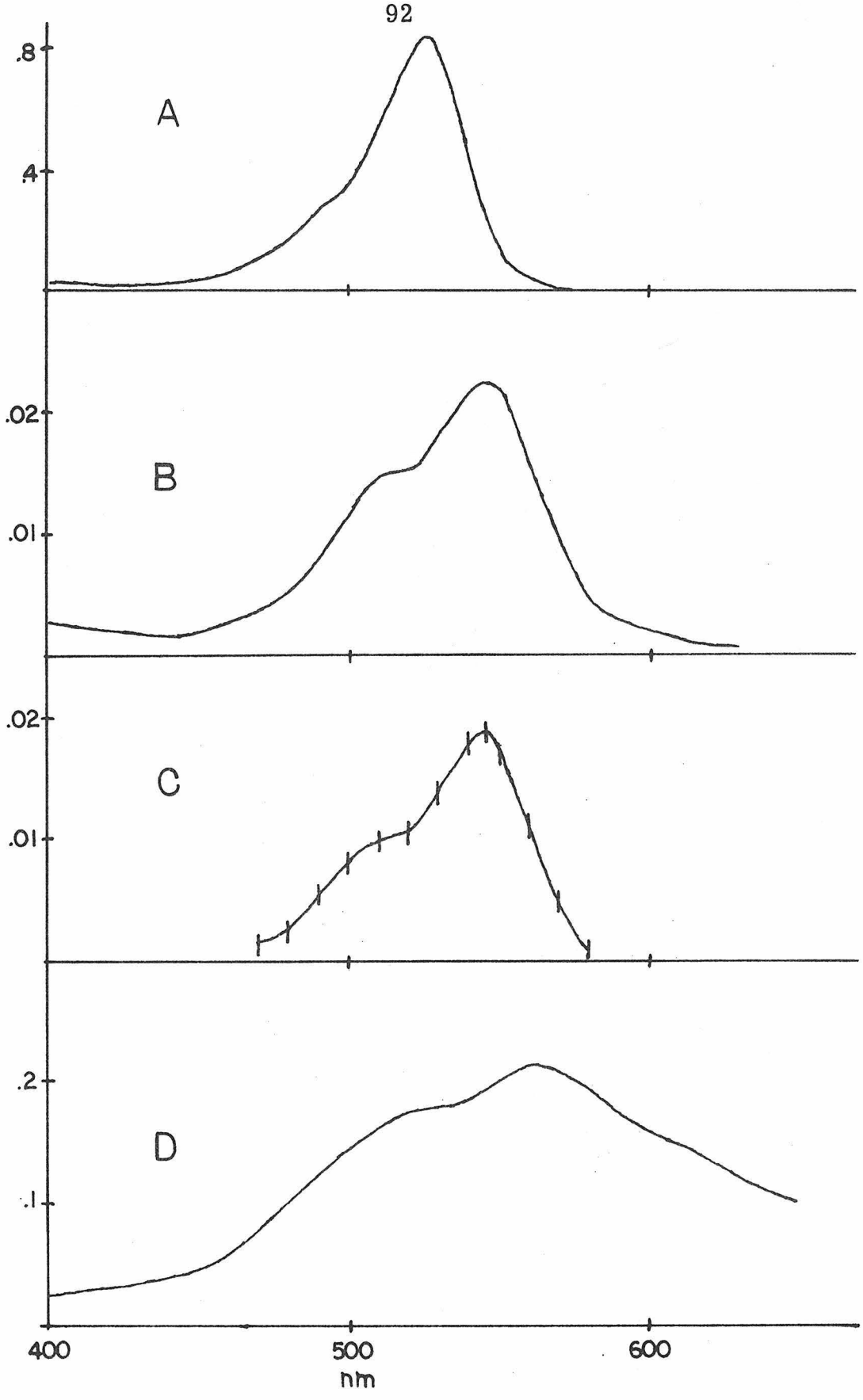
.8
A
.4
.02
B
.01
.02
C
.01
.2
D
.1
400
500
600
nm

cm (within a factor of 2), the surface concentration was calculated to be 2×10^{-10} moles/cm^2, comparable to an estimated monolayer coverage (1.0×10^{-10} moles/cm^2). The absorbance was observed to increase slowly with longer exposures to the solution; for example, a quartz disc soaked for 5 minutes in a 10^{-3} M solution produced a maximum absorbance 20% higher than when it was exposed for only 1 minute. Furthermore, for a given exposure time, the absorbance was dependent on the solution dye concentration, being lower for lower concentration. The low accuracy of the measurements precluded any fit to a theoretical isotherm; however, the surface concentration appeared to saturate at high dye concentrations.

The nature of the adsorbed RH6G layer is, of course, important for the mechanism of sensitization. The absorption peak was red-shifted roughly 20 mμ, or 660 cm^{-1}. Bathochromism immediately rules out structures containing well-defined dimers or higher aggregates, because these forms exhibit hypsochromism, i.e., blue-shifted bands [33]. A special form of aggregation does lead to a new narrow absorption band at longer wavelengths, referred to as the J band [33]. Pseudoisocyanine (Fig. II-3) and related compounds very frequently display this type of behavior. The J-aggregate can function as an efficient sensitizing species [14]. However, J-aggregation appears to require a compact stacking of the molecules, and

rhodamine dyes, with the twisted phenyl group, are not expected to form structures with the necessary transition dipole coupling. A further argument against the assignment of the 545 mμ peak as a J-band lies in the broadness of that peak, totally uncharacteristic of a J-band. The bathochromic shift might be explained by adsorption onto the substrate. West and Geddes [34] have shown that a good correlation exists between absorption maxima shifts and the index of refraction of the solvent or the solid substrate; a larger index of refraction resulted in a red shift. This explanation seems unlikely in this case because the same peak position is observed on quartz ($n = 1.46$) and SnO_2 ($n = 2.0$) [21].

The broadness of the adsorbed layer spectrum and its similarity to the monomer spectrum leads to the hypothesis that each molecule is interacting very weakly with neighboring dye molecules, which have no special orientation, or at least are not stacked with parallel dipole oscillators. The adsorbed layer structure may be approaching that of the RH6G crystal. A Nujol mull spectrum (Fig. II-20) shows even broader bands and a larger red shift. The shoulder on the higher energy side may be due to an enhancement of a higher vibronic transition; its position in all of the spectra is approximately 1000 cm^{-1} above the absorption maximum. One remaining inconsistency is the slight difference between the adsorbed layer absorption peak and the

wavelength of peak sensitization. A luminescence study of the adsorbed layer would be desirable, but no detectable emission was observed in the Perkin-Elmer Fluorescence Spectrophotometer. As crystalline RH6G is itself only weakly luminescent at room temperature, another attempt at liquid nitrogen temperatures is suggested.

The effects of dye concentration upon the photocurrent were investigated in three distinct wavelength regions. The SW (short wavelength) region referred to wavelengths between 350 and 400 mμ, where the high background photocurrent was presumed to dominate. The hypothesis was that any slow changes in the background photocurrent due to lamp intensity drift, accidental displacement of the cell, etc. could be monitored by changes in the photocurrent in this region. No concentration dependence was expected to show up in the SW region. The DW (dye wavelength) region included wavelengths near the absorption peak of RH6G. Finally, the LW wavelengths were sufficiently long to completely avoid any light absorption by the monomer, even for a 33 mμ bandwidth in the excitation light. Although LW photocurrents were approaching the noise limitations, these wavelengths were also expected to furnish calibration for the background photocurrent.

To facilitate comparison of photocurrents for different experiments, a ratio plotting method was adopted. The photocurrent at a

given λ and dye concentration was divided by the background photocurrent at that λ, which was measured prior to the first addition of dye. Errors introduced by variations in the cell position between experiments were eliminated in this fashion. The change in the photocurrent due to the dye alone, referred to as the corrected photocurrent, was calculated by subtracting 1 from the ratio.

In Fig. II-21, the photocurrent concentration dependence for increasing concentration in water is shown. The dye-sensitized photocurrent rose gradually over a broad concentration range, but even at the lowest concentrations some sensitization was evident in agreement with the spectral observation of adsorbed dye layers even from dilute ($< 10^{-5}$ M) dye solutions. The background photocurrent, characterized by the SW measurements, remained constant within ±10%. Surprisingly, the LW photocurrents started increasing at the highest concentrations. Since the dye in the bulk solution was not absorbing light at those wavelengths, and cutoff filters removed higher order spectra from the monochromator output, the increased light absorption in the LW region is probably due to formation of the adsorbed layer; in Fig. II-20, it is evident that adsorption leads to a broadened, red-shifted band with increased light absorption above 600 mμ.

Fig. II-21. Concentration Dependence in Water

⊙ -- total dye concentration

△ -- monomer concentration

⊡ -- point obtained by dilution

The electrolyte was 0.2 M NaF/H_2O. The vertical axis is linear with the logarithm of the ratio (see text).

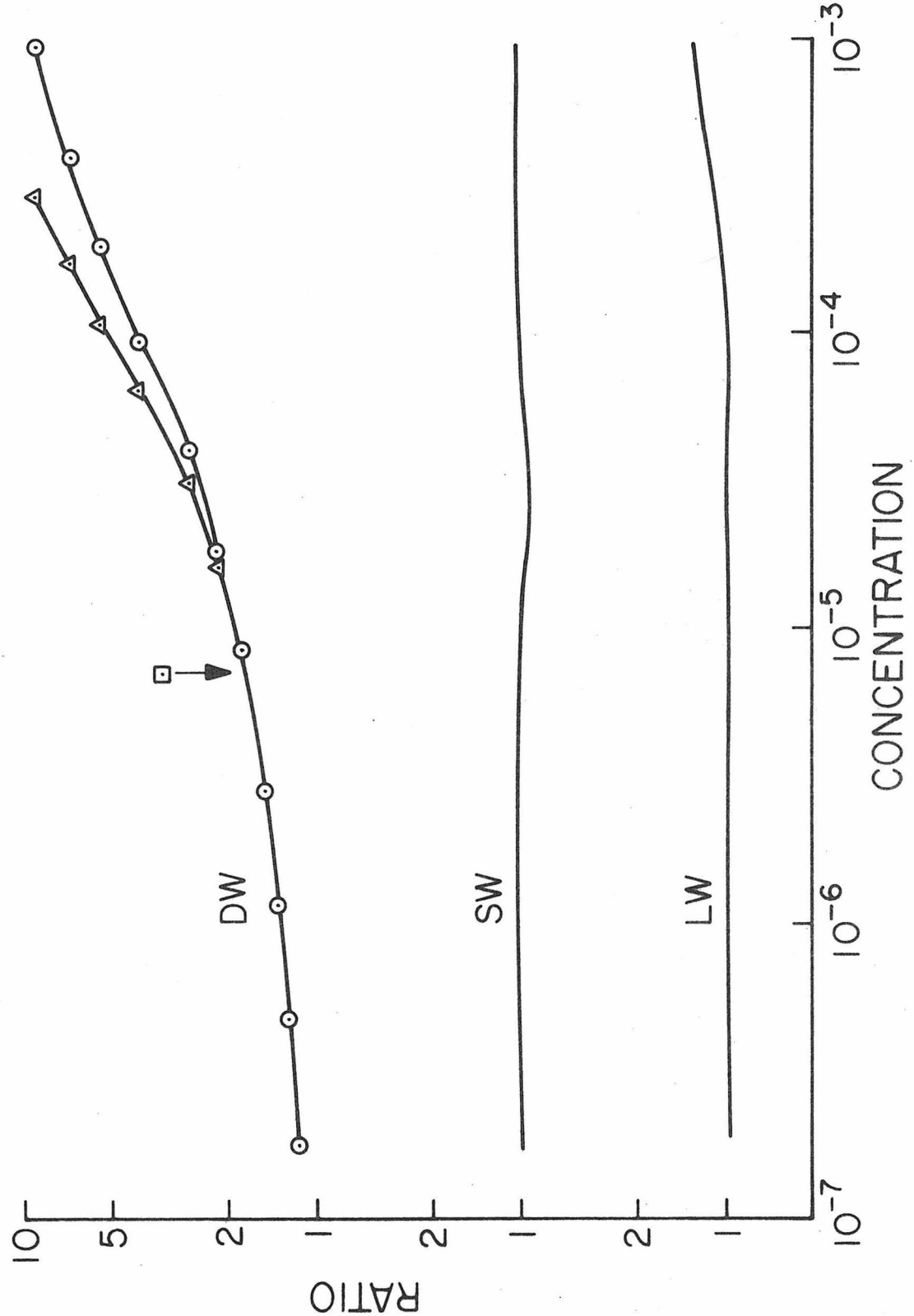
10
5
2
1
2
1
2
1
RATIO
DW
SW
LW
10^{-7}
10^{-6}
10^{-5}
10^{-4}
10^{-3}
CONCENTRATION

In Fig. II-22, the corrected photocurrent (ratio - 1) is compared with Laitinen's results for polycrystalline SnO_2 electrodes [16]. Although Laitinen did not correct for the background photocurrent, this curve could be obtained from his graphs. Two differences are evident: the enormously greater sensitization factor, and the generally steeper slope for Laitinen's data. The difference could possibly be attributed to the technique of electrode preparation. Laitinen's electrodes could have a much lower density of intermediate and surface states, resulting in the greater sensitization factor. However, qualitatively the background photocurrent spectra are very similar. A lower intermediate state density would result in a much steeper drop in background photocurrent at photon energies just below the band gap. Another possibility is that the carrier concentration is much lower in Laitinen's electrodes. However, no one to date has experimentally demonstrated a correlation between either of these two factors and degree of sensitization by dyes. One could also argue that rhodamine B is strongly chemisorbed by the carboxylate bond, whereas RH6G is only physically adsorbed. To check this point, the behavior of the photocurrent was measured at intervals of 10-15 minutes after each addition of dye. After the maximum dye concentration had been reached, the solutions were diluted to check the reversibility of the adsorption process.

Fig. II-22. Corrected Photocurrent Concentration Dependence in Water

A -- vs. total concentration; from ref. 16

B -- vs. total concentration; calculated from Fig. II-21.

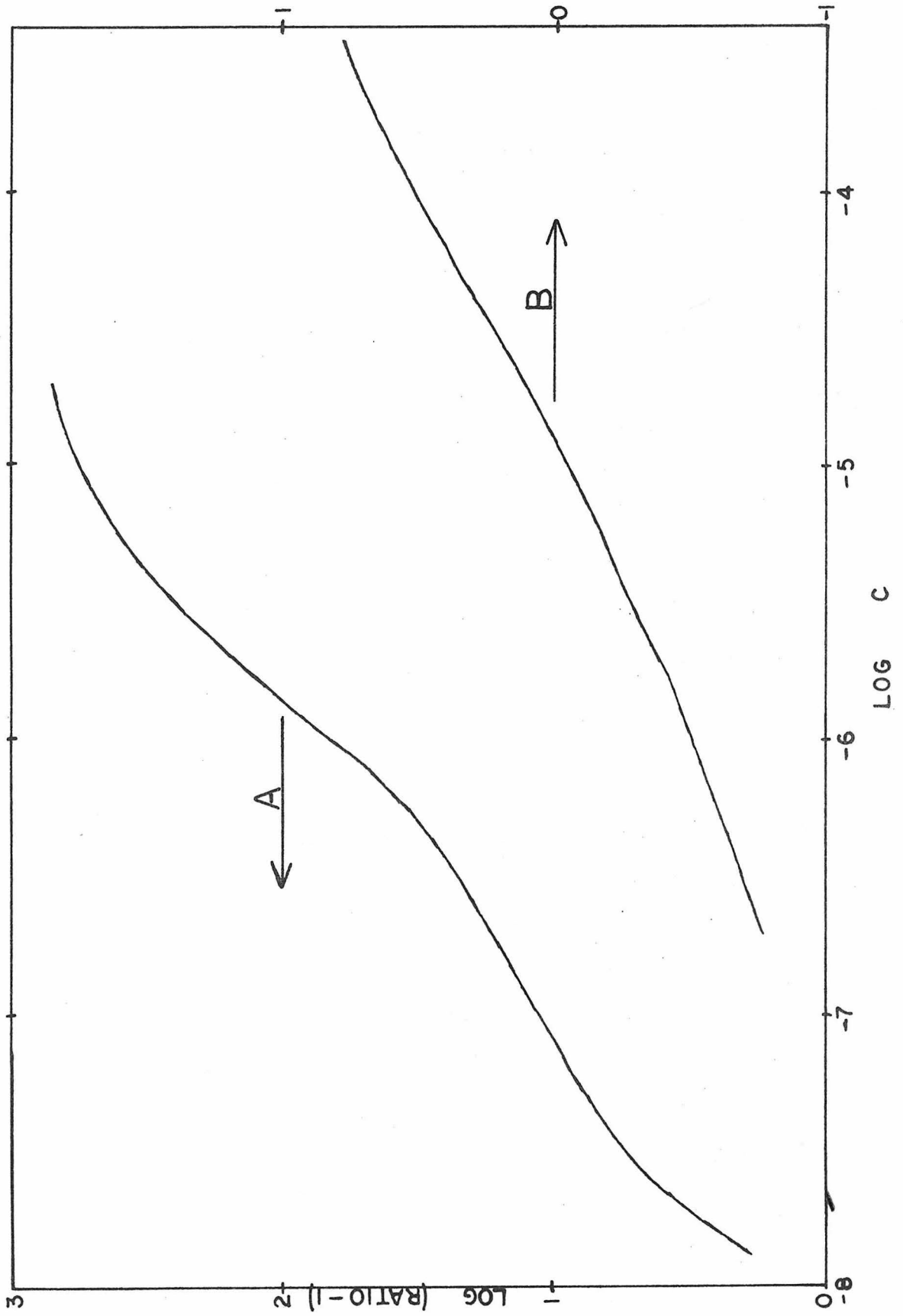
LOG (RATIO - 1)
LOG C
A
B
3
2
1
0
-1
-2
-3
-4
-5
-6
-7
-8

The photocurrents at SW and DW were observed to slowly increase with time after the initial measurement, but at the higher concentrations ($> 10^{-5}$ M), the percentage increase at DW (4-5% per 15 minute inverval) exceeded the increase at SW (1-2%). Upon dilution, the DW photocurrents showed an immediate drop in magnitude, but these data points were consistently higher than the line drawn through the data points obtained with increasing concentration. This hysteresis was especially noticeable when the bulk of the dye-electrolyte solution was replaced with pure electrolyte; the boxed data point in Fig. II-21 was obtained in this manner. Furthermore, the overall magnitude of the photocurrent decreased slowly with subsequent measurements after dilution. This behavior indicated slow adsorption and desorption process. Chemisorption, of course, can account for the irreversibility, the chemisorption process being the hydrolysis of the ethyl ester on RH6G followed by bonding to the surface hydroxides. The dye molecules could be slowly diffusing into fissures in the electrode surface. The slow thickening of the surface layer observed via spectra is also consistent with this behavior. However, the results obtained in acetonitrile (vide infra) indicate that an occlusion or chemisorption mechanism is more likely.

The slope of the log (corrected photocurrent) versus log (concentration) plot is considerably less than 1, especially at the

lowest concentrations. The lack of proportionality to concentration, which deviates from other concentration studies [7, 12, 16], may be due to the effect of the semiconductor surface structure on the structure of the adsorbed layer. The rather low sensitization factor in these experiments may also be explained by the nature of the dye-semiconductor interface structure. For example, the dye layer could be localized clumps, with the effective concentration of molecules actually adjacent to the semiconductor being much lower than in a uniform monolayer. It is not clear whether the abscissa should be log total concentration or log monomer concentration, i.e., how do solution dimers affect the formation of the adsorbed layer?

Sensitized photocurrent densities of well over 100 nA/cm^2 were obtained at the highest concentrations. For a photon flux of 10^{16} photons/sec/cm^2, this corresponds to a quantum yield of 0.01, where $\phi = 1$ implies one electron injected into the semiconductor for every photon absorbed by a dye monolayer. Because only 1/100 of a monolayer is consumed per second, consumption of dye is not rate-determining in the decay of the photocurrent with time.

In acetonitrile several striking differences appeared in the concentration study (Fig. II-23). In the DW region, dye sensitization did not appear to start until concentrations between 10^{-4} M and 10^{-3} M were reached. Surprisingly, the SW photocurrent actually decreased

Fig. II-23. Concentration Dependence in Acetonitrile
0.1 M TEAP/CH_3CN, Ratio Plot

The boxed data points ⊡ were obtained by dilution from the highest concentration.

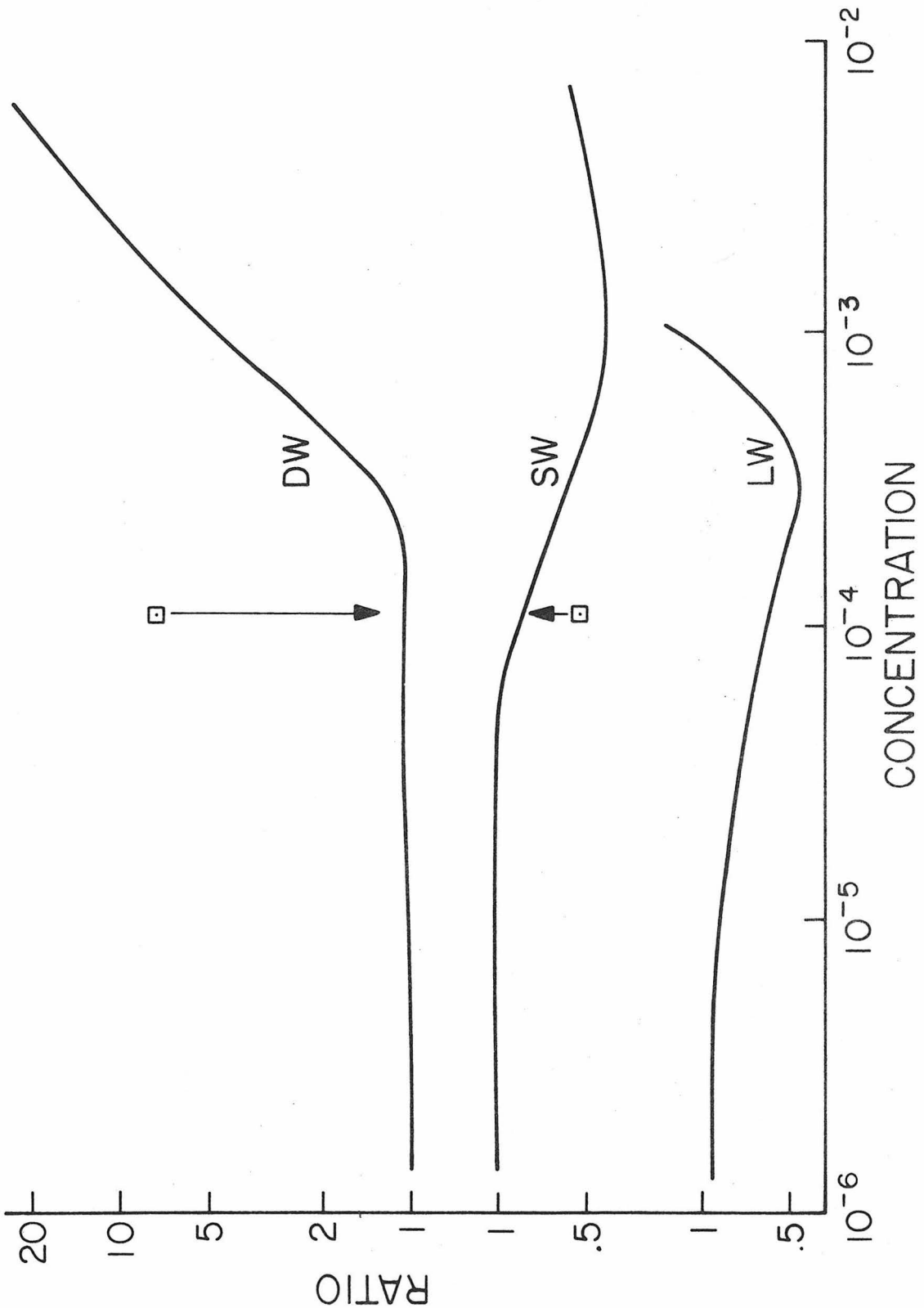
DW
SW
LW
20
10
5
2
1
1
.5
1
.5
RATIO
10^{-6}
10^{-5}
10^{-4}
10^{-3}
10^{-2}
CONCENTRATION

by roughly a factor of two between 10^{-4} and 10^{-3} M, and then started increasing again. The onset of SW photocurrent suppression and the dye sensitization occurred at roughly the same concentration (10^{-4} M). As was noted in water, the LW photocurrents followed the SW photocurrents except at the higher dye concentrations, where a strong sensitization effect appeared. Photocurrent spectra with and without dye are shown in Fig. II-24.

If one assumes that the background photocurrent mechanism is dominant in the SW region, at least for concentrations less than 10^{-3} M, then the presence of the dye must be inhibiting the rate of electron injection into available holes. The most likely process is the lowering of the concentration of oxidizable species at the semiconductor surface. The major differences between water and acetonitrile solutions are the absence of dimers and the absence of an insoluble adsorbed layer in the latter solvent. Dye layers deposited from aqueous solutions are rapidly removed in acetonitrile and alcohols. The background photocurrent suppression curve resembles an isotherm, suggesting the formation of an adsorbed layer. In view of the solvation of thick layers in CH_3CN, it seems likely that only a compact monolayer of dye is deposited. Because the much smaller water molecules are displaced, the surface concentration of hole acceptor is decreased.

Fig. II-24. Dye-Sensitized Photocurrent Spectrum
RH6G in Acetonitrile

——— 0.1 M TEAP/CH_3CN

- - - 1.0×10^{-3} M RH6G

+0.71 V vs. SCE

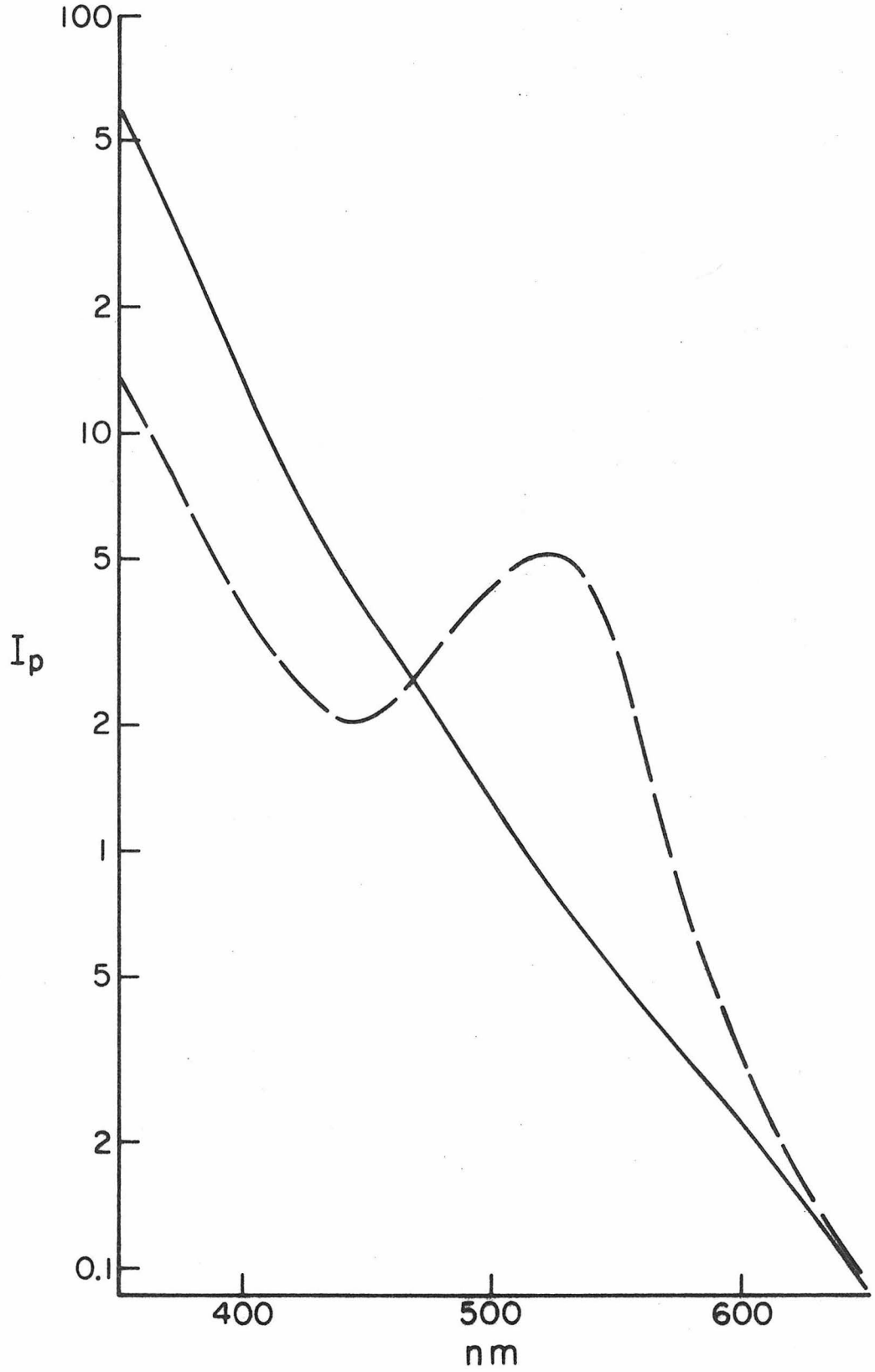
100
5
2
10
5
2
1
5
2
0.1
I_p
400
500
600
nm

Why, then, was the same effect not observed in water? The photocurrent time decay and history dependence in H_2O was similar with and without dye, even at the maximum photocurrent densities of 10^{-6} A/cm^2, indicating that transport of charge and/or ions between the electrode and bulk solution must not be seriously hampered. As was suggested above, the dye molecules could be adsorbed in clumps, with sufficient interstitial space to allow water molecules to diffuse to the electrode and oxidized products to diffuse out. The "clump" hypothesis certainly agrees with the micellar adsorption proposed earlier[19].

If the background photocurrent is assumed to be uniformly suppressed at all wavelengths, then the photocurrent due to dye only may be calculated by subtracting the SW ratios from the DW ratios at each concentration. The resulting curve (Fig. II-25) has a steeper slope than the equivalent one in water; the dye-sensitized photocurrent is roughly proportional to dye concentration. Again, maximum sensitized photocurrent densities were greater than 100 nA/cm^2, although higher dye concentrations were required to attain this level.

The suppression of the SW photocurrents stopped at 10^{-3} M, suggesting the completion of a monolayer. The SW photocurrent then started to rise, and the DW photocurrent continued to rise up to the saturation concentration of the dye. At 10^{-3} M, the concentration of

Fig. II-25. Corrected Photocurrent Concentration Dependence

A -- 0.2 M NaF/H_2O

B -- 0.1 M $TEAP/CH_3CN$

C -- unity slope

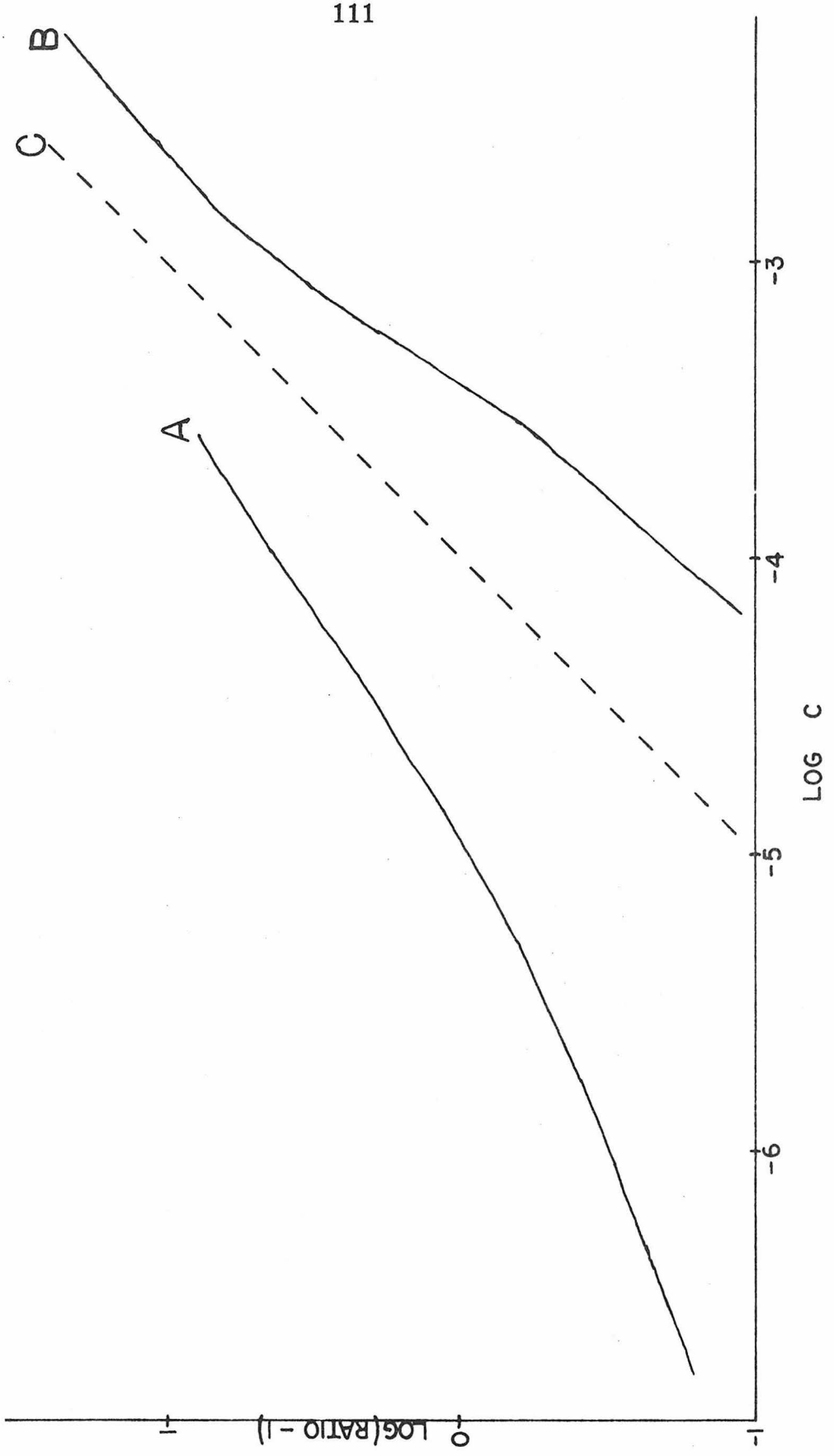
B
C
A
-3
-4
-5
-6
LOG C
-1
0
1
LOG(RATIO - 1)

RH6G molecules within 10 Å of the surface is roughly 100 times lower than the surface concentration of a monolayer; thus, it is conceivable that at these concentrations molecules not adsorbed or chemisorbed could contribute to the sensitized photocurrent. The continuous rise in sensitization represents the first piece of evidence that this process may occur.

However, the dye-sensitized photocurrent exhibited the same history-dependent behavior in acetonitrile as in water. At concentrations above 10^{-4} M, subsequent measurements at DW yielded photocurrents 5 to 15% higher than the initial value. Dilution of the solution produced photocurrents at both DW and SW which corresponded to much higher concentrations on the initial curve. This irreversible behavior points to the necessity of a chemisorption or an occlusion process to sensitize photocurrents.

Several possibilities for further work exist. Other dyes without a carboxylate group should be investigated for irreversible behavior, e.g., methylene blue. Interaction with the surface charge can be elucidated by using anionic, cationic, and neutral dyes. A concentration study using $Ru(bipy)_3^{2+}$ as a sensitizer would be interesting because of its non-planar geometry and long-lived excited state. The polycrystalline SnO_2 electrode should be compared with a single crystal electrode, especially with respect to the magnitude of

sensitization photocurrents. Finally, the effects of carrier concentration and/or intermediate levels on the magnitude of sensitization should be determined.

One possible method for determining the molecular state involved in the sensitized photocurrent mechanism is to monitor the fluorescence of the adsorbed dye layer as a function of electrode potential. Because the quantum yield of photocurrent increases for increasing potential positive of the flat-band potential (Fig. II-13), fluorescence of the adsorbed layer should decrease concomitantly, if the singlet excited state of the dye is the state from which an electron is transferred to the semiconductor.

To selectively excite the adsorbed layer, the technique of total internal reflection (TIR) was used[24, 25]. Light totally reflected off of the electrode-solution interface (Fig. II-9) creates an evanescent wave in the solution phase which decays exponentially with distance from the electrode:

$$I = I_0 \exp\left(-\frac{z}{d}\right)$$

I_0 is the evanescent intensity at the interface, z the distance from the interface, and d is the effective penetration depth calculatable by the expression[25]:

$$d = \frac{\lambda}{4\pi (n_1^2 \sin^2 \theta - n_3^2)^{1/2}}$$

n_1 is the index of refraction of the electrode substrate (quartz), n_3 the index of refraction of the solution phase (assumed to be the same as the pure solvent), and θ the angle of incidence of the exciting beam, measured relative to the normal to the interface. TIR is only accomplished at angles above the critical angle $\theta_c = \sin^{-1} (n_3/n_1)$, which for the quartz-water or quartz-acetonitrile systems is $\sin^{-1}$ (1.34/1.46) = 66.6°. It should be noted that this is slightly above the 65° prism angle, requiring rotation of the cell plus prism to a slightly higher angle of incidence. Optical constants of any intermediate phases, such as the tin-oxide layer, do not enter into the expression for d. At angles slight above the critical angle, where I_0 is maximum, d is approximately 150 mμ for wavelengths used to excite RH6G. This distance is small enough that even at the highest dye concentrations used (10^{-2} M), evanescent wave intensity is only dependent on the equation given above and not on absorption losses. One can also calculate that at 10^{-3} M, a monolayer of adsorbed dye would absorb 5 times as much light as molecules in the solution. If fluorescence quantum efficiency is not affected by adsorption, then most of the fluorescence emission observed would originate in the monolayer.

Unfortunately, ϕ_f is apparently affected by adsorption, as was noted in the earlier discussion on the dye layers deposited from water. Fluorescence was not completely quenched, however, as faint emission was visually detectable from more concentrated layers formed on rough silica surfaces.

Another factor which made detection of monolayer fluorescence difficult was light scattering. Figure II-26 illustrates the anomalous behavior obtained for dyes in nonaqueous solvents. At the highest concentration, the excitation spectrum closely resembled the absorption spectrum of rhodamine B even though the curves were uncorrected for excitation beam intensity (I_0) at the interface. I_0 is a complex function of excitation beam intensity and the optical constants of the quartz substrate, the SnO_2 layer, and the solution, all of which are wavelength dependent; apparently these factors interact to produce a reasonably uniform I_0 in the 400-600 mμ region. A very similar excitation spectrum was obtained in a standard fluorescence cell using very low dye concentration and conventional excitation geometry. The excitation spectrum followed the absorption spectrum because ϕ_f is independent of exciting wavelength over the entire absorption band[35]. At lower concentrations, gross distortion of the excitation spectrum was observed.

Fig. II-26. Excitation Spectra in the TIR Mode

Rhodamine B in ethanol; angle of incidence = 68-70°; 8 mμ bandpass for the excitation and emission monochromator. For excitation, monitoring wavelength = 610 nm, for emission, exciting wavelength = 515 nm. Relative instrument response for a constant signal shown by arrows.

A -- 10 m<u>M</u>; dashed curve is fluorescence spectrum

B -- 1 m<u>M</u>

C -- 0.1 m<u>M</u>

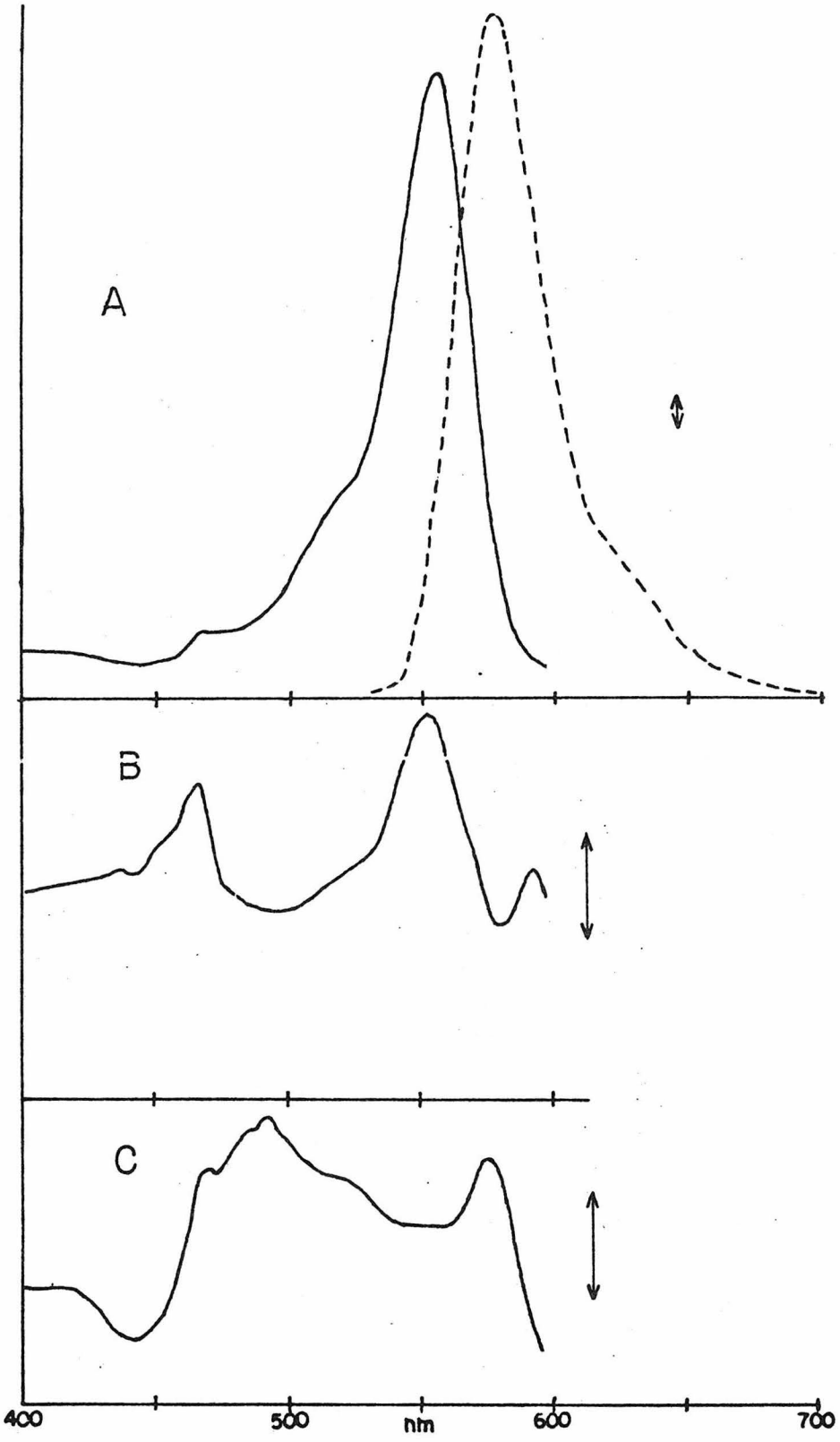
A
B
C
400
500
nm
600
700

Light from a scattering center within the prism or the SnO_2 electrode frequently approaches the electrode-solution interface at an angle below θ_c, and hence passes through the interface. This light penetrates far into the solution, exciting many more dye molecules than an evanescent wave of comparable intensity. The emission spectrum of fluorescence excited by scattered light is nearly identical to fluorescence excited by the evanescent wave, but large differences appear in the excitation spectrum due to geometrical factors inherent to the design of the fluorescence spectrophotometer. Emission from the cell is collected by a lens and focused onto the entrance slit of the emission monochromator. Any shift in the position or shape of the emitting region causes large fluctuations in the amount of light passing through that entrance slit. Light scattered into the solution produces an emitting region that changes irregularly with wavelength, both by increased scattering at shorter wavelengths and by increased penetration depths at wavelengths less strongly absorbed by the dye. In contrast, the evanescent wave restricts the emission to such a thin layer of solution that its shape is effectively constant with respect to the collecting lens at all wavelengths.

A more subtle effect also distorts excitation spectra. Consider a well-designed spectrophotometer in which emission is physically confined such that geometrical distortions do not occur.

The rate of emission of fluorescence, Q, is equal to the rate of light absorption multiplied by the fluorescence quantum efficiency.

$$Q = I_a \phi_f$$

I_a can be determined by measuring the intensity of the light entering and leaving the cell, which in turn can be calculated from Beer's Law.

$$I_a = I_0 - I = I_0(1 - 10^{-\epsilon bc})$$

$$Q = I_0 \phi_f (1 - 10^{-\epsilon bc}) \qquad (1)$$

If the solution absorbance ϵbc is small, i.e., < 0.01, then

$$Q = I_0 \phi_f (2.3\ \epsilon bc) \qquad (2)$$

All the parameters in Equation (2) are independent of excitation wavelength except ϵ, so that a true excitation spectrum is obtained. As the solution absorbance increases, it becomes necessary to use Equation (1), and at high absorbances the fluorescence becomes saturated at a constant determined by I_0 and ϕ_f; the excitation spectrum becomes a straight line. Below this extreme, excitation spectra peaks are found to be relatively lower than the corresponding absorption spectra peaks. Note that in the evanescent wave region, the rate of light absorption

is given by

$$I_a = I_0 \epsilon C \int_0^{\infty} \exp(-z/d)dz = I_0 \epsilon c d$$

so that

$$Q = I_0 \phi_f \epsilon cd$$

Thus, undistorted excitation spectra[36] are only obtained from molecules excited by the evanescent wave, and not by scattered light. Figure II-26 demonstrates that light-scattering interference prevents the observation of fluorescence from dye layers adjacent to the electrode at concentrations below 10^{-3} M; the rhodamine B absorption peak disappears at lower concentrations.

A further complication arose in water; dimer formation led to strong fluorescence quenching[37]. Despite this difficulty, the conclusive result was that no potential dependence of the TIR-excited fluorescence was observed in aqueous or acetonitrile electrolytes. The only condition that affected emission intensity was the onset of dye reduction at very negative potentials. The most likely explanation of this negative result lies in the low quantum yield of the sensitized photocurrent. Less than 1/100 of the photons absorbed by a monolayer are converted to current; variations in the emission intensity of such a small fraction of the molecules would have very little effect

on the overall measured intensity, especially if most of the fluorescence was coming from molecules not adsorbed onto the electrode. A more ideal system for these experiments would be dyes with high fluorescence quantum yields adsorbed on single-crystal semiconductor electrodes, where photocurrent quantum yields approaching 1 have been reported[8].

REFERENCES

1. H. Kuhn, J. Chem. Phys., 53, 101 (1970).
2. R. R. Chance, A. Prock, and R. Silbey, J. Chem. Phys., 60, 2184 (1974).
3. Ibid., 60, 2744 (1974).
4. H. Tributsch and H. Gerischer, Ber. Bunsenges. Physik. Chem., 73, 850 (1969).
5. H. Gerischer and H. Tributsch, Ber. Bunsenges. Physik. Chem., 72, 437 (1968).
6. H. Gerischer, M. E. Michele-Beyerle, F. Rebentrost, and H. Tributsch, Electrochim. Acta, 13, 1509 (1968).
7. H. Tributsch and H. Gerischer, Ber. Bunsenges. Physik. Chem., 73, 251 (1969).
8. H. Gerischer, Photochem. Photobiol., 16, 243 (1972).
9. R. Memming and H. Tributsch, J. Phys. Chem., 75, 562 (1971).
10. R. Memming, Photochem. Photobiol., 16, 325 (1972).
11. H. Tributsch, Photochem. Photobiol., 16, 261 (1972).
12. K. Hauffe, H. J. Danzmann, H. Pusch, J. Range, and H. Volz, J. Electrochem. Soc., 117, 993 (1970).
13. U. Bode, K. Hauffe, Y. Ishikawa, and H. Pusch, Z. Physik. Chem. N. F., 85, 144 (1973).

14. H. Tributsch, Ber. Bunsenges. Physik. Chem., 73, 582 (1969).

15. R. Memming, Far. Soc. Symposia, 8 (1974) in press.

16. H. Kim and H. A. Laitinen, J. Electrochem. Soc., 122, 53 (1975).

17. K. Hauffe and U. Bode, Far. Soc. Symposia, 1974, in press.

18. K. H. Drexhage, Topics in Appl. Phys., 1, 144 (1973).

19. M. M. Allingham, J. M. Cullen, C. H. Giles, S. K. Jain, and J. S. Woods, J. Appl. Chem., 8, 108 (1958).

20. H. Gerischer, Surf. Sci., 18, 97 (1969).

21. T. Arai, J. Phys. Soc. Japan, 15, 916 (1960).

22. K. Ishiguro, T. Sasaki, T. Arai, and I. Imai, J. Phys. Soc. Japan, 13, 296 (1958).

23. F. Möllers and R. Memming, Ber. Bunsenges. Physik. Chem., 76, 469 (1972).

24. N. J. Harrick, "Internal Reflection Spectroscopy", Interscience, 1967.

25. W. N. Hansen, Adv. Electrochem. Electrochem. Eng., ed. Delahay and Tobias, 9, 1 (1973).

26. H. Gerischer, Physical Chemistry, ed., H. Eyring, 9A, 463 (1970).

27. H. Gerischer, Adv. Electrochem. Electrochem. Eng., 1, 139 (1969).

28. M. Green, Modern Aspects Electrochem., ed., J. O'M. Bockris, 2, 343 (1959).

29. C. Kittel, "Introduction to Solid State Physics", John Wiley and Sons, Inc., 4th ed., 1971, pp. 361-395.

30. T. Freund and S. R. Morrison, Surf. Sci., 9, 119 (1968).

31. R. A. Vanden Berghe and W. P. Gomes, Ber. Bunsenges. Physik. Chem., 76, 481 (1972).

32. H. Gerischer and E. Meyer, Z. Physik. Chem. N. F., 74, 302 (1971).

33. J. Nys, "Dye Sensitization--Symposium Bressanone", ed. by W. F. Berg, U. Mazzucato, H. Meier, and G. Semerano, Focal Press, London, 1970, pp. 26-43 and references cited therein.

34. W. West and A. L. Geddes, J. Phys. Chem., 68, 837 (1964).

35. C. A. Parker, "Photoluminescence of Solutions", Elsevier Publishing Co., Amsterdam, 1968, p. 247.

36. d is proportional to λ, enhancing emission at longer wavelengths. The effect on the qualitative features of the spectra is small.